Universiteit Utrecht

Koninklijk Nederlands Meteorologisch Instituut
Ministerie van Infrastructuur en Waterstaat

Ocean Dynamic Sea Level Projections During the 21st Century Along the Dutch Coast

An Analysis of CMIP5 and CMIP6

MASTER THESIS

Franka T.F. Jesse
Climate Physics

Supervisors:
Dr. D. Le Bars
Royal Netherlands Meteorological Institute (KNMI)
Prof. dr. S.S. Drijfhout
Royal Netherlands Meteorological Institute (KNMI)
Institute for Marine and Atmospheric research Utrecht (IMAU)
Prof. dr. H.E. de Swart
Institute for Marine and Atmospheric research Utrecht (IMAU)
July 2022

Abstract

One of the major contributors to sea level rise along the Dutch coast during the 21st century is Ocean Dynamic Sea Level (ODSL). ODSL is defined as the sea level anomaly due to ocean currents, wind stresses and local thermosteric and halosteric effects. Along the Dutch coast, climate models project an ODSL rise between 0 - 35 cm at the end of the century, depending on the emission scenario. Hence, this accounts for a large part of the total projected sea level rise of 30 - 120 cm along the Dutch coast. It is important that climate models are able to model ODSL correctly. However, the current state-of-the-art climate models from CMIP5 and CMIP6 show a large spread in ODSL projections and ODSL rise at the Dutch coast increased significantly between CMIP5 and CMIP6. One hypothesis for the latter is the larger increase in global mean temperature in CMIP6. This increase is larger than the assessed ranges provided in the Sixth Assessment Report (AR6) by the Intergovernmental Panel on Climate Change. In this study, we aim to improve the quality of ODSL projections from CMIP5 and CMIP6 by better understanding the processes that influence ODSL change along the Dutch coast. First, we use linear regression models to identify the reason for a model's ODSL change. The processes we consider as explanatory variables for ODSL change are global surface air temperature (GSAT), global mean thermosteric sea level (GMTSL), and the Atlantic meridional overturning circulation (AMOC) strength. Using only GSAT as a predictor variable works for the CMIP5 ensemble but does not explain all long-term changes for CMIP6. Including an additional predictor variable improves the model. More specifically, we find that the model using predictor variables GSAT and AMOC performs best at predicting ODSL change at the Dutch coast for both CMIP5 and CMIP6. For most individual models, we find that an increase in GSAT, and a weakening of the AMOC, relate to an increase in ODSL along the Dutch coast. The regression analysis results are combined with Monte Carlo sampling to generate probabilistic ensembles of ODSL projections consistent with the AR6 assessed ranges of GSAT and GMTSL. This method enables us to correct the ODSL change for the high temperature bias in CMIP6 models. We find that the effect of GSAT is too small to explain the difference in ODSL between CMIP5 and CMIP6. However, we see that the sensitivity to GMTSL and AMOC increased in CMIP6 which could point to a difference in model dynamics between CMIP5 and CMIP6. Furthermore, we find that the location of deep convection is important for ODSL along the Dutch coast. We see that models that show a deep mixed layer in the Greenland Sea for the period 1975 - 2004, project a larger rise in ODSL at the Dutch coast for both ensembles.

Contents

List of Acronyms

AMOC . . . . . Atlantic meridional overturning circulation
AR6 . . . . . Sixth Assessment Report
CMIP5 . . . . . Coupled Model Intercomparison Project Phase 5
CMIP6 . . . . . Coupled Model Intercomparison Project Phase 6
GMSL . . . . . Global mean sea level
GMTSL . . . . . Global mean thermosteric sea level
GSAT . . . . . Global surface air temperature
IPCC . . . . . Intergovernmental Panel on Climate Change
ODSL . . . . . Ocean dynamic sea level

1 Introduction

1.1 Global and Regional Sea Level Rise

Sea level rise is one of the main consequences of global warming. The rise of global mean sea level (GMSL) has accelerated over the past decades due to thermal expansion of sea water and an increased mass loss of land ice. Recently, Steffelbauer et al., 2022 showed that this acceleration is also observed along the Dutch coast. Projections show that GMSL will continue to rise during the 21st century as a consequence of anthropogenic forcing (Slangen et al., 2016; Oppenheimer et al., 2019; Fox-Kemper et al., 2021). The rise of sea level has a broad socio-economic and environmental impact on coastal communities and low-lying countries (Hinkel et al., 2014). Among the most vulnerable regions are countries such as China, Vietnam, and Indonesia (Dasgupta et al., 2009), but also in Europe, more than 200 million citizens live within 50 km from the coastline (Vousdoukas et al., 2020). Because of this large impact, it is of significant importance to provide policymakers with reliable projections that can serve as the basis for implementing adequate adaptation measures.

In some areas, sea level rise is projected to be larger than in others and therefore, the projections in sea level are not spatially homogeneous. These regional differences arise mainly from three processes: (1) ocean dynamics, (2) rotational and gravitational effects caused by redistribution of mass within the cryosphere and hydrosphere, and (3) vertical land motion caused by glacial isostatic adjustment (Stammer et al., 2013). Along the Dutch coast, ocean dynamics is one of the major contributors to total sea level rise during the 21st century. The rise of sea level due to ocean dynamics is referred to as ocean dynamic sea level (ODSL). ODSL is defined as the sea level deviation from the geoid, with the inverse barometer effect applied (Gregory et al., 2019). A simpler way of explaining ODSL is that it reflects the sea level anomaly due to local thermosteric and halosteric effects, ocean currents and wind stresses (Gill and Niller, 1973; Gregory et al., 2016). The interannual variability in ODSL is large, mainly due to wind effects. By definition, the global mean of ODSL is zero.

1.2 Ocean Dynamic Sea Level in Global Climate Models

The primary tools to construct ODSL projections are atmosphere-ocean general circulation models (AOGCMs). The Coupled Model Intercomparison Project (CMIP) is a standard experimental framework for studying the output of coupled AOGCMs developed by groups worldwide. Figure 1.1 shows the median ODSL change at the end of the century projected by the latest two phases from CMIP (CMIP5 and CMIP6). For these results, the models were forced with an intermediate emission scenario. The temporal average over 2081 - 2100 is compared to the reference period 1900 - 1949. The spatial patterns in CMIP5 and CMIP6 are similar and most of the larger-scale features are reasonably well understood. For instance, the rise of ODSL in

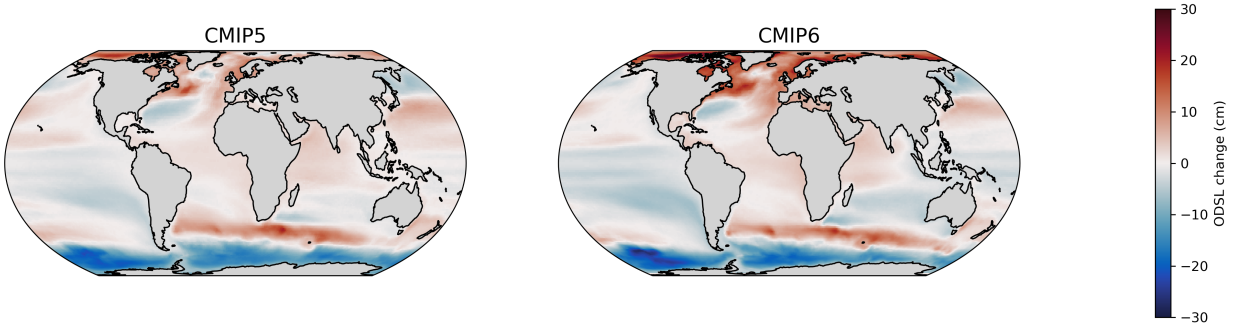

Figure 1.1: Ensemble median ODSL change in CMIP5 and CMIP6 from model runs forced with an intermediate emission scenario (RCP4.5 for CMIP5, and SSP2-4.5 for CMIP6). The difference between 2081 - 2100 and reference period 1900 - 1949 is shown. These results are based on 27 models for CMIP5, and 30 for CMIP6.

the Arctic is driven by increased freshwater input (Couldrey et al., 2021), and the meridional dipole pattern in the North Atlantic is driven by a reduction in heat loss north of 40°N (Bouttes et al., 2014). The difference between CMIP5 and CMIP6 is most pronounced at higher latitudes and in the Arctic. In these regions, CMIP6 models project a larger rise of ODSL. The results are similar for the other emission scenarios.

The ODSL pattern near the European coast is shown in Figure 1.2. The North Sea is one of the regions that show larger increase in ODSL, together with the area along the Norwegian coast and North and West of the British Isles. This is found for the lower and higher emission scenarios as well. Furthermore, the difference between CMIP5 and CMIP6 is similar to the sea level change patterns themselves. This indicates that the pattern from CMIP6 models is amplified with respect to CMIP5. This is also the case for the other emission scenarios.

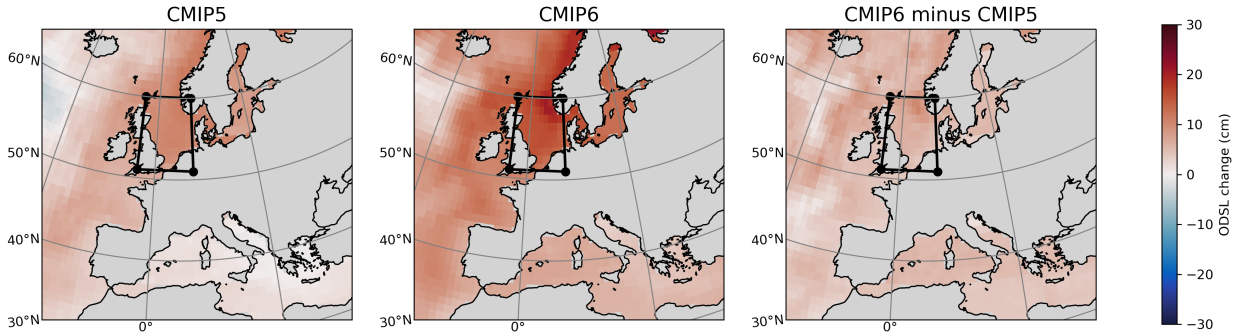

Figure 1.2: Ensemble median ODSL change for the intermediate emission scenario. The difference between 2081 - 2100 and reference period 1900 - 1949 is shown for CMIP5 (left) and CMIP6 (centre), and the difference between CMIP5 and CMIP6 is plotted (right). The North Sea region is indicated with black lines.

In this study, the focus is on long-term ODSL change along the Dutch coast. Instead of only selecting grid cells near the Dutch coast, we consider changes over the North Sea, indicated by the black box in Figure 1.2. One motivation for this is that global climate models are not always able to resolve small scale processes sufficiently. For instance, some models show checkerboard-like patterns for ODSL in the North Sea (Hermans et al., 2020). We filter these spatial inaccuracies by taking the average over a larger region. The choice is validated by the fact that steric effects are expected to be similar for the North Sea and the

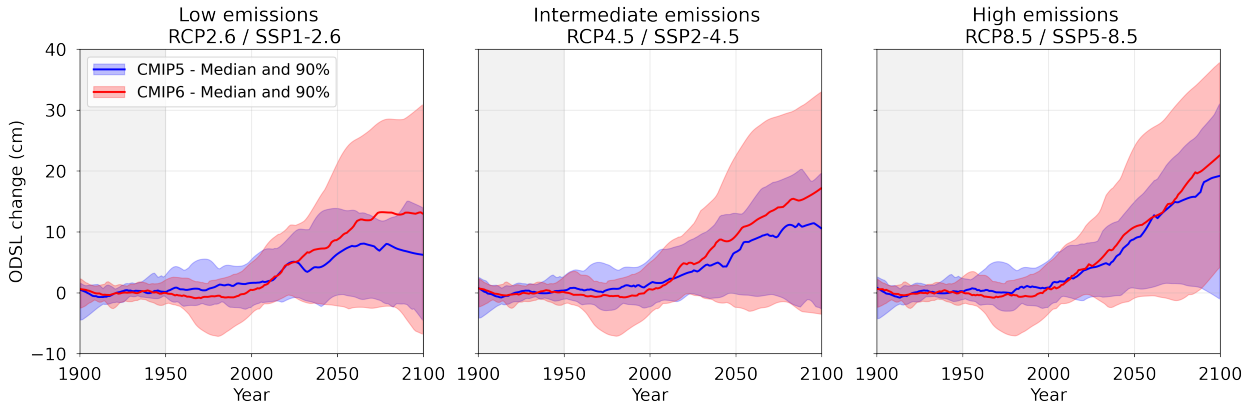

Figure 1.3: ODSL projections for the North Sea from CMIP5 (blue) and CMIP6 (red) models for three scenarios: low emission scenario RCP2.6/SSP1-2.6, intermediate emission scenario RCP4.5/SSP2-4.5, and high emission scenario RCP8.5/SSP5-8.5. The median and the 5 - 95 percentile of the ensembles are plotted. The reference period (1900 - 1949) is indicated by grey shading.

Dutch coast since most of the steric increase is due to overflow from the deep ocean (Bingham and Hughes, 2012). This overflow is expected to be distributed homogeneously over the basin. Furthermore, by taking the average over the North Sea, we filter out some of the highly variable wind effects. The smoothed time series of the spatially averaged ODSL in the North Sea are shown in Figure 1.3 for three different emission scenarios[1]. The CMIP5 ensemble shows a slight positive trend for all scenarios during the 20th century, followed by a faster rise between 2000 - 2075 and a drop after 2075 for the low and intermediate emission scenarios. The CMIP6 ensemble shows no rise in ODSL during the 20th century, followed by a fast rise starting in 2000. For the low and intermediate scenarios, the rise slows down in 2060. Note that the uncertainty bands show a dip in ODSL change between 1960 and 2000 for the CMIP6 ensemble. This is not seen in the CMIP5 time series.

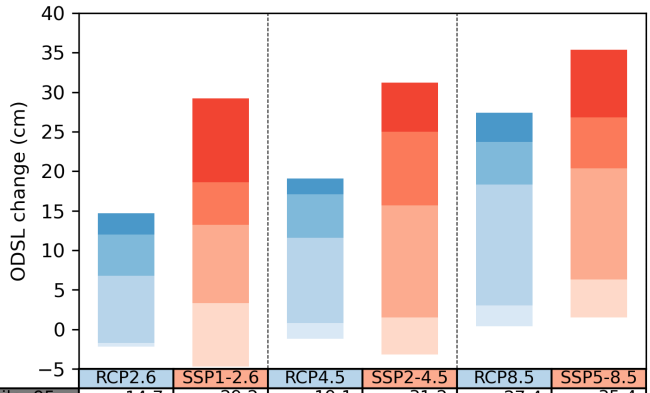

	RCP2.6	SSP1-2.6	RCP4.5	SSP2-4.5	RCP8.5	SSP5-8.5
Percentile: 95	14.7	29.2	19.1	31.2	27.4	35.4
Percentile: 83	12.0	18.6	17.1	25.0	23.7	26.8
Percentile: 50	6.8	13.2	11.6	15.7	18.3	20.4
Percentile: 17	-1.7	3.3	0.8	1.5	3.0	6.3
Percentile: 5	-2.2	-4.7	-1.2	-3.2	0.4	1.5

Figure 1.4: ODSL change in the North Sea region between 2081 - 2100 and 1900 - 1949 for three scenarios for CMIP5 (blue) and CMIP6 (red). The edges of the bars represent the different percentiles given in the table.

Figure 1.4 summarises the end of the century projections of ODSL in the North Sea for the lower, intermediate, and higher emission scenarios for both CMIP5 and CMIP6. The projected change averaged over 2081 - 2100 is plotted for different percentiles of the ensemble. Compared to the period 1900 - 1949, climate models thus predict an ODSL rise of 0 - 35 cm along the Dutch coast at the end of the 21st century, depending on the emission scenario. This accounts for a large part of the total projected sea level rise of 30 - 121 cm along the Dutch coast (KNMI, 2021). Two other things stand out from this Figure. First, we note that the CMIP6 ensemble shows a larger spread in the projections for the lower and intermediate emission scenarios. This is surprising since we would expect the additional development time of the models to reduce the divergence. Second, we see that CMIP6 models project a larger ODSL change than CMIP5 models for all scenarios. Previous studies show that changes in ODSL can be related to changes in global temperature (Perrette et al., 2013; Yuan and Kopp, 2021; Bilbao et al., 2015). Remarkable is that the climate sensitivity of the CMIP6 models is higher, leading to higher global mean temperatures. This is also referred to as the 'hot model' problem (Zelinka et al., 2020; Hausfather et al., 2022), and could thus potentially play a role in the increased ODSL rise in CMIP6. The sixth assessment report (AR6) of the Intergovernmental Panel on Climate Change (IPCC) provides assessed temperatures ranges for each scenario. These ranges are lower than the CMIP6 temperature ranges, and for most scenarios higher than the CMIP5 temperature ranges (see Appendix A). The primary aim of this study is to correct for these assessed temperatures and investigate if this reduces the difference between the ensembles, and the uncertainty in the projections.

[1]The emission scenarios are represented by Representative Concentration Pathways (RCPs) in CMIP5, and by Shared Socioeconomic Pathways (SSPs) in CMIP6. The scenarios considered in this study are low emissions (RCP2.6 / SSP1-2.6), intermediate emissions (RCP4.5 / SSP2-4.5), and high emissions (RCP8.5 / SSP5-8.5)

1.3 Difficulty of Observing Ocean Dynamic Sea Level

One might think that another way to reduce the uncertainty in the projections is to constrain them with observations. However, directly measuring the change in ODSL is not possible. One way to estimate it is by subtracting all known contributions from the total sea level rise, which is measured by tide gauges and satellites. The remaining part is then due to the change in ODSL. This method's disadvantage is that the propagation of uncertainty in the other contributors leads to large uncertainty in the remaining ODSL. Another way to estimate the past change in ODSL is to use reanalysis data of temperatures and atmosphere. A third way makes use of the reasoning by Bingham and Hughes, 2012, stating that steric increase in shallow seas can be computed using the steric increase in the deep ocean nearby. The effects of the wind are not included in these steric budgets. Figure 1.5 compares the time series of two steric budgets (Steric 1 and Steric 2), ORA 20-C reanalysis data and the individual CMIP models. A smoothing filter is applied to the latter two to exclude the variability caused by wind effects. The reference period is set at 1980 - 1999 as all time series cover this period. For the reanalysis, ten individual members and the mean are plotted. We see that the members show a large spread in the first half of the 20th century. Furthermore, the reanalysis data shows a significant drop in ODSL in 1950. This drop is not seen for Steric 2 and neither for most of the CMIP models. If we look at the period from 2000 and on, we see that the reanalysis data shows a faster rise than the budgets. Summarising, we find that the different budgets and reanalysis data do not agree well. Therefore, it is not possible to constrain the projections with observations. This motivates us to get a better understanding of the ODSL data from the CMIP models which could help us decrease the uncertainty in the projections.

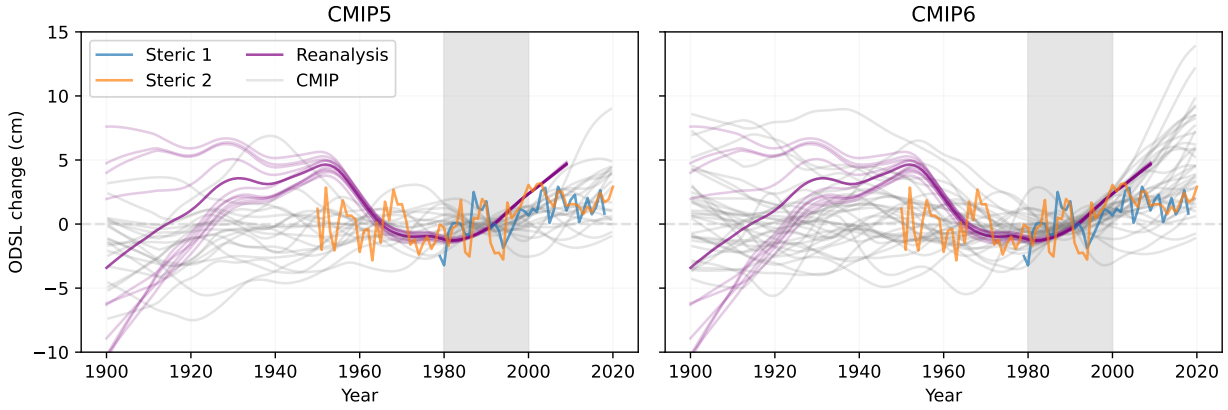

Figure 1.5: ODSL time series for the Dutch coast from ORA-20C reanalysis data (purple) covering 1900 - 2009, Steric 1 covering 1979 - 2018 (blue), Steric 2 (orange) covering 1950 - 2020, and individual CMIP models (grey) covering 1900 - 2020. A smoothing window of 25 years is used for the reanalysis and CMIP data to filter out the short-term effects of the wind. No smoothing window is applied to the steric budgets since these are not influenced by wind. The grey shading indicates the reference period from 1980 - 1999.

1.4 Previous Studies on Ocean Dynamic Sea Level

Since we cannot make any model selection based on the budgets and reanalysis, we need to work with the CMIP data as it is. In order to correct the data for the assessed AR6 temperatures, we have to get a better idea of what processes drive the long-term (multidecadal) change in ODSL along the Dutch coast. Here, we provide a short overview of earlier work.

Several studies use pattern scaling[2] approaches to relate ODSL change to certain climate variables. Perrette

[2]Pattern scaling is a simple way to produce climate projections beyond the scenarios run with AOGCMs. The technique assumes that a spatial climate anomaly pattern obtained from an AOGCM can be scaled by a global climate variable (Tebaldi and Arblaster, 2014).

et al., 2013 derive a spatial pattern by regressing ODSL on global mean surface air temperature (GSAT). Bilbao et al., 2015 examined the relationship between ODSL and GSAT, global mean thermosteric sea level (GMTSL), ocean volume mean temperature, and global mean sea surface temperature using pattern scaling. They find that ocean volume mean temperature is generally a better predictor than GSAT. Additionally, they show that the pattern is very similar under different scenarios for a given model. Palmer et al., 2020 present a new set of local sea level projections based on CMIP5 using global thermal expansion (GTE) as regressor for ODSL. Yuan and Kopp, 2021 build upon Bilbao et al., 2015's speculation about the relative importance of shallow and deep warming under different scenarios and develop an emulator for ODSL change using GSAT and deep ocean temperature as predictor variables. The time series for GSAT and deep ocean temperature are generated based on emulation of five individual CMIP5 models using a two-layer model, FaIR-2LM. By combining the time series with the regression coefficients and using Monte Carlo sampling, they construct probabilistic ensembles of ODSL projections. This method allows them to interpolate between emission scenarios and propagate the uncertainty at low computational costs.

The main conclusion of the pattern scaling studies discussed above is that it is possible to scale the pattern of ODSL with global climate variables. Multiple studies however point to the importance of local processes that could influence ODSL. For instance, for the North Atlantic, several studies relate ODSL change with the strength of the Atlantic meridional overturning circulation (AMOC). Katsman et al., 2008 found that a significant reduction of the AMOC correlated with larger steric sea level in the eastern North Atlantic basin using CMIP3 models. Chen et al., 2019 find that the large uncertainty in CMIP5 ODSL projections in the North Atlantic is connected to the uncertainty in the change of the AMOC. They suggest that reducing the inter-model spread in the change of the AMOC can greatly improve the consistency of ODSL projections among different models. Lastly, Lyu et al., 2020 analyse ODSL data from CMIP5 and CMIP6 and find that the larger ODSL change in the North Atlantic in CMIP6 is associated with a larger weakening of the AMOC.

Since the North Sea is part of the North Atlantic, we expect that the AMOC influences ODSL levels at the Dutch coast as well. Therefore, we expect that including the AMOC as a predictor variable in the pattern scaling method could be an improvement.

1.5 Research Questions

The primary aim of this study is to obtain ODSL projections that are consistent with the AR6 assessed ranges of GSAT and GMTSL and to see if this correction explains the difference between CMIP5 and CMIP6. We formulate the following research questions:

1. *What processes can be related to ocean dynamic sea level change along the Dutch coast?*
2. *Can the difference in predicted temperature increase between CMIP5 and CMIP6 models explain the difference in ocean dynamic sea level change?*
3. *Can we provide ocean dynamic sea level projections that are consistent with the AR6 assessed ranges of temperature and global mean thermosteric sea level?*

The data is discussed in Section 2, together with information on the different emission scenarios and the assessed ranges of GSAT and GMTSL from the AR6. To answer the first question, we use (multiple) linear regression models discussed in Section 3.1 including the predictor variables: GSAT, GMTSL, and AMOC. The latter is included since earlier research points out that the AMOC is related to ODSL in the North Atlantic. Therefore we expect it to also be of importance for the North Sea. In order to make the projections consistent with the AR6 assessed ranges, we combine the regression coefficients with Monte Carlo sampling to generate probabilistic ensembles of ODSL. This method is primarily inspired by Yuan and Kopp, 2021 and further discussed in Section 3.2. Using the corrected projections, we will find an answer to question 2. as well. The results are presented in Section 4, followed by the discussion in Section 5. Finally, we answer our research questions in 6.1, and provide some suggestions for further research in 6.2.

2 Data

This study uses global climate model data, observations and reanalysis data, and assessed ranges from the AR6.

2.1 CMIP5 and CMIP6 Model Data

For the analysis of the processes that can be related to ODSL, we use Phase 5 (CMIP5) and Phase 6 (CMIP6) data from the Coupled Model Intercomparison Project. The models included in CMIP all run a long spin-up simulation using stationary forcings. The pre-industrial control (piControl) simulation branches out from the spin-up and uses fixed forcings. Analysing the piControl run allows us to diagnose the climate drift in an unforced system. The historical simulation branches out of the spin-up at the same time and covers the years 1850 - 2005 for CMIP5, and 1850 - 2014 for CMIP6. In these simulations, all time-varying climate forcings known for this period are used (e.g. greenhouse gases, volcanic activity, solar radiation).

The future projections use the end of the historical experiment as the initial conditions and run until 2100 for most models. Future projection runs are forced with different greenhouse gas scenarios. These scenarios are reflected by Representative Concentration Pathways (RCPs) in CMIP5 as defined by Van Vuuren et al., 2011, and by Shared Socioeconomic Pathways (SSPs) in CMIP6 as defined in O'Neill et al., 2014. We focus on three different scenarios in this study: low radiative forcing (RCP2.6 / SSP1-2.6), intermediate radiative forcing (RCP4.5 / SSP2-4.5), and high radiative forcing (RCP8.5 / SSP5-8.5).

We select the models that provide data for ODSL and GSAT. Some of these models also provide data for GMTSL and AMOC. An overview of the number of models that have data available for given combinations of variables is given in Table 2.1. The complete list of models and their institutes can be found in Appendix B. For each model, only the first ensemble member indicated by the ensemble name *'r1i1p1'* is used. For all variables, we obtain the yearly average from the downloaded monthly data, and we set the reference period to 1900 - 1949. The next subsections contain more detailed information about the post-processing steps of the individual climate variables.

		ODSL + GSAT	ODSL + GSAT + GMTSL	ODSL + GSAT + AMOC
CMIP5	RCP2.6	20	18	7
	RCP4.5	27	23	8
	RCP8.5	25	21	9
CMIP6	SSP1-2.6	30	19	14
	SSP2-4.5	30	20	14
	SSP5-8.5	31	20	15

Table 2.1: Number of models available for each combination of variables for the different scenarios and CMIP phases.

2.1.1 Ocean Dynamic Sea Level

ODSL is given by the CMIP variable *zos*. It has three dimensions: time, latitude, and longitude. The piControl simulation is used to correct for the linear drift in each model's historical and future scenario simulations (Hobbs et al., 2016). The models do not discretise the ocean on identical grids. To be able to analyse the models together, the data is regridded to the same $1.0° \times 1.0°$ grid. Besides, the land-sea mask is not the same for all models. This causes issues close to the coast and in almost enclosed seas. By spatially extrapolating the available data to where there is no data, we avoid having spatial discontinuities in maps of the ensemble mean and standard deviation. ODSL at the Dutch coast is obtained by taking the spatial average over the region indicated by the black box in Figure 1.2 (51.5°N – 59.5°N, 3.5°W – 7.5°E).

2.1.2 Global Mean Thermosteric Sea Level

GMTSL is given by the CMIP variable *zostoga*. Similar to *zos*, the linear drift in *zostoga* is removed using the piControl runs. Furthermore, some models from CMIP5 showing non-physical discontinuities in *zostoga* are filtered out.

2.1.3 Global Surface Air Temperature

GSAT is given by the CMIP variable *tas*. The global mean of the *tas* variable is downloaded from the KNMI Climate Explorer (*Climate Explorer* n.d.). The drift of the data in the piControl run was found to be small. Therefore, the GSAT data has not been corrected for this.

2.1.4 Atlantic Meridional Overturning Circulation

As a proxy for the AMOC strength we use the overturning mass stream function, given by *msftmyz* in CMIP5, and by *msftmz* for the meridional direction or *msftyz* for the y-direction in CMIP6. No drift correction is performed for these variables. We take the stream function at latitude 26°N, which is the latitude often used in literature (Cunningham et al., 2007; Mielke et al., 2013). The stream function is then divided by the average density of ocean water, $\rho = 1026$ kg/m^3, and multiplied by 10^{-6} to obtain the AMOC strength in Sverdrups (Sv). For CMIP6, some models provide data for both variables *msftmz* and *msftyz*. *msftmz* is used when it is available for a certain model, otherwise we take *msftyz*.

2.2 Observational and Reanalysis Data

2.2.1 Ocean Dynamic Sea Level

This section contains some background on the reanalaysis and budget data for ODSL that was shown in Section 1.3. Ocean Reanalysis of the 20th Century (ORA-20C) is a 10-member ensemble of ocean reanalyses covering the past century (*Ocean Reanalysis of the 20th Century — ECMWF* n.d.). The data set has a spatial resolution of $1.0° \times 1.0°$. It uses atmospheric forcing from ERA-20c, ECMWF's first atmospheric reanalysis of the 20th century. We use variable *zos* from the ORA-20C data set. Monthly data for this variable is available from January 1900 to December 2009. For the analysis, we obtain the annual average and use a smoothing filter of 15 years.

Additionally, we compare two local steric budgets with the reanalysis and CMIP data. These budgets are computed by integrating changes in temperature and salinity at deep-ocean sites close to the Dutch coast. The first budget, 'Steric 1', covers the years 1979 - 2018 and uses EN4 data (Good et al., 2013). Temperature and salinity differences are integrated down to 4000 m. The second budget, 'Steric 2', covers 1950 - 2020 and uses IAP data (*Ocean and Climate* n.d.). Integration goes down to 1100 m.

2.2.2 Global Surface Air Temperature

Observations of GSAT are used for the reconstructions and taken from the HadCrut5 data set (*Met Office Hadley Centre observations datasets* n.d.). We use variable *tas*. The best estimate and 2.5 - 97.5 percentile are provided and we use data from 1900 to 2005.

2.2.3 Global Mean Thermosteric Sea Level

There are no direct observations of GMTSL change as it is one of several contributors to total sea level change. Frederikse et al., 2020b obtain an estimate of GMTSL over the past century based on in situ subsurface observations and reconstructions by Zanna et al., 2019. The data from 1900 to 2005 is used and obtained via Frederikse et al., 2020a. We use the best estimate and the 5 - 95 percentile.

2.3 AR6 Assessed Ranges

The AR6 presents assessed ranges for future GSAT and GMTSL under different emission scenarios. These are used to make the ODSL projections for the 21st century consistent with the AR6 GSAT and GMTSL ranges for the lower (SSP1-2.6), intermediate (SSP2-4.5), and higher (SSP5-8.5) emission scenario.

2.3.1 Global Surface Air Temperature

The assessed ranges for GSAT are given in Chapter 4.3.4, Table 4.5 of AR6 WG1 (Lee et al., 2021). These assessed future changes are explicitly constructed by combining scenario-based projections with observational constraints based on past simulated warming. Best estimates and 5 - 95 percentile values for each scenario are given for three periods: 2021 - 2040, 2061 - 2080, and 2081 - 2100. A third-order polynomial is fitted to these values to obtain yearly values. The left panel in Figure 2.1 shows the observational data for GSAT combined with the AR6 assessed changes for the three scenarios this study focuses on.

2.3.2 Global Mean Thermosteric Sea Level

The assessed ranges for global mean steric sea-level ranges are obtained from NASA's Sea Level Change Portal (*Sea Level Projection Tool – NASA Sea Level Change Portal* n.d.). The assessed global mean thermosteric sea level rise is derived from a two-layer energy budget emulator consistent with the assessment of ECS and TCR (Fox-Kemper et al., 2021). Ranges are given for every ten years. The best estimate and 5 - 95 percentile values are used, and again a third-order polynomial is fitted to the values to obtain assessed ranges for each year. The right panel in Figure 2.1 shows the reconstructed GMTSL data from Frederikse et al., 2020b combined with the AR6 assessed ranges.

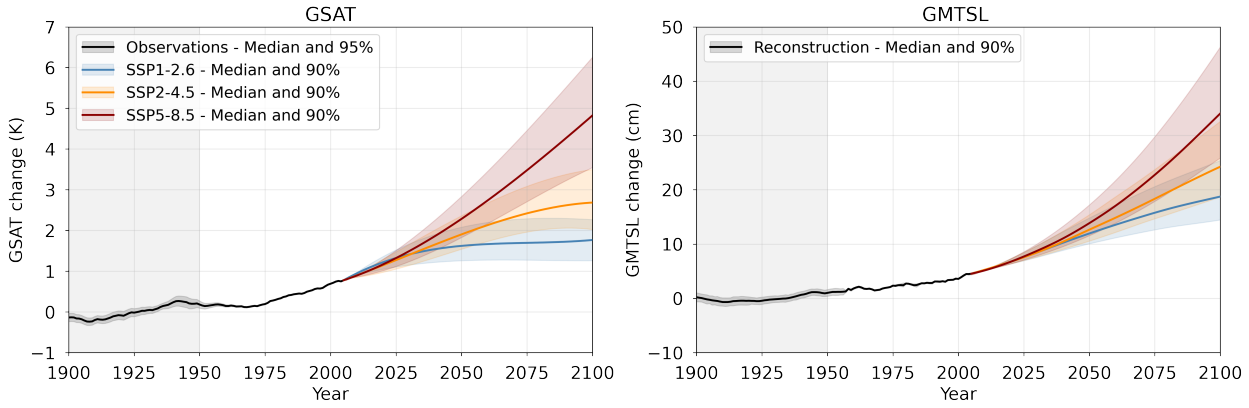

Figure 2.1: GSAT and GMTSL time series of the obersvational product, and the assessed AR6 ranges for different scenarios. For the GSAT observations, the ensemble median and the 2.5 - 97.5 percentile from the HadCrut5 dataset are shown. For GMTSL, the ensemble median and 5 - 95 percentile from the reconstructions based on Frederikse et al., 2016 are shown. The AR6 ranges cover the period 2005 - 2100, and the ensemble median and 5 - 95 percentile are shown. Grey shading denotes the reference period 1900 - 1949.

3 Methods

3.1 Investigating the Possible Drivers of ODSL

To find the answer to our first research question, and inspired by aforementioned studies (Perrette et al., 2013; Bilbao et al., 2015; Palmer et al., 2020; Yuan and Kopp, 2021), we analyse the relation between ODSL and different variables using (multiple) linear regression models. The three predictor variables we consider are global surface air temperature (GSAT), global mean thermosteric sea level (GMTSL), and the strength of the Atlantic meridional overturning circulation (AMOC). The regression analysis uses time series from the individual CMIP5 and CMIP6 models. For each model, we obtain scenario-independent scaling factors between ODSL and the different variables. In the following sections, smoothing of the data, three different regression models, and the method of analysing their performance are presented.

3.1.1 Data Smoothing

The interannual variability in ODSL is relatively large, mainly due to wind effects. We are, however interested in the longer-term change in ODSL. In order to exclude the short-term variability we use a locally weighted scatterplot smoothing (LOWESS) filter. This method fits separate regression to fragments of the data. The window size of the fragments is set at 25 years. The LOWESS filter is applied to all variables from the CMIP data sets, and the reanalysis data.To give a better idea on the amount of interannual variability in ODSL and GSAT, the time series for the CanESM5 model is plotted in the upper panel of Figure 3.1. The lower panel shows the smoothed time series using the 25-year LOWESS filter.

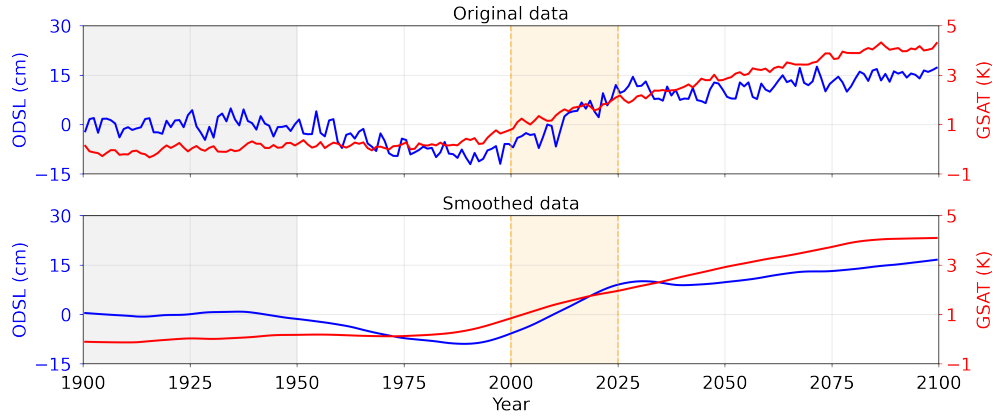

Figure 3.1: Comparison of original and LOWESS smoothed data for ODSL (blue) and GSAT (red) from CMIP6 model 'CanESM5'. The grey area denotes the reference period, and the orange area shows the window size used for the smoothing.

3.1.2 Model I: GSAT as Predictor

The first regression model (Model I) is a simple linear regression model with predictor variable GSAT. This choice is motivated by the fact that ODSL is affected by changes in temperature and salinity, which are themselves affected by changes in (among others) surface fluxes of heat (Lowe and Gregory, 2006; Bouttes and Gregory, 2014). The regression model is defined as

$$\mathrm{ODSL}(t) = \alpha + \beta_G \times \mathrm{GSAT}(t) + \epsilon(t), \tag{1}$$

where α is an intercept term which can be interpreted as the offset, β_1 is the regression coefficient which can be interpreted as the scaling relationship between ODSL and GSAT, and ϵ is the residual term. We make the assumption that the sensitivity of ODSL to GSAT is similar under different scenarios. To obtain the scenario-independent regression coefficients for each model, we concatenate the historical time series of

ODSL and GSAT with the time series from the available scenario runs. Using these concatenated time series, the regression analysis is performed for all individual models from CMIP5 and CMIP6 that have ODSL and GSAT data available.

3.1.3 Model II: GSAT and GMTSL as Predictors

The second model (Model II) includes GMTSL as an additional regressor for ODSL. This variable depends on the interior redistribution of heat and therefore on the three-dimensional temperature field within the ocean. This variable thus reacts on different time scales than GSAT. This regression model is expressed by

$$\text{ODSL}(t) = \alpha + \beta_1 \times \text{GSAT}(t) + \beta_2 \times \text{GMTSL}(t) + \epsilon(t). \tag{2}$$

This model is identical to Model I except for the third term, which represents the contribution of GMTSL to ODSL with regression coefficient β_2. Again, we perform the analysis with the concatenated time series of the historical run and the available scenario runs for each model separately.

3.1.4 Model III: GSAT and AMOC as Predictors

Several studies comment on the importance of the AMOC on ODSL in the North Atlantic (Katsman et al., 2008; Lyu et al., 2020). This motivates us to investigate the relation between the AMOC and ODSL in the North Sea in our third model (Model III). Also, including a local process like the AMOC might improve the predictive power of the model. We thus include AMOC as an additional predictor variable and define the third model as

$$\text{ODSL}(t) = \alpha + \beta_1 \times \text{GSAT}(t) + \beta_2 \times \text{AMOC}(t) + \epsilon(t). \tag{3}$$

3.1.5 Analysis of Regression Models

The Root Mean Squared Error (RMSE) estimates the deviation of the regression model results from the actual data. This metric can thus be used to evaluate and compare the performance of the regression models. The RMSE is computed for each CMIP model separately by taking the sum of the squared residual term for each time step. Mathematically we can define it as

$$\text{RMSE}_j = \sqrt{\frac{1}{N}\sum_{k=1}^{N} \epsilon_j(t_k)^2}, \tag{4}$$

where subscript j denotes the model, N is the number of data points, in our case, the available years for the data, and $\epsilon_j(t_k)$ is the residual term at time t_k. The better the fit of our regression model, the smaller the residual term and therefore also the smaller the RMSE. To study the general performance of the regression model for the complete ensembles, we obtain the ensemble average RMSE for CMIP5 and CMIP6 by taking the average of the RMSE of the individual models.

3.2 Generating Probabilistic ODSL Ensembles

To answer the last two research questions, we use the results from the regression analysis to generate probabilistic ensembles of ODSL projections for both CMIP5 and CMIP6. Our method is primarily inspired by Yuan and Kopp, 2021, in which they combine the regression coefficients with Monte Carlo sampling. We generate two types of ensembles. For the first type, the input data for the explanatory variables is based on the CMIP data. We call this type of ensemble the 'CMIP ensemble'. The second type of ensembles uses input data for GSAT and GMTSL based on observations and the assessed ranges of AR6. We call this the 'AR6 ensemble'.

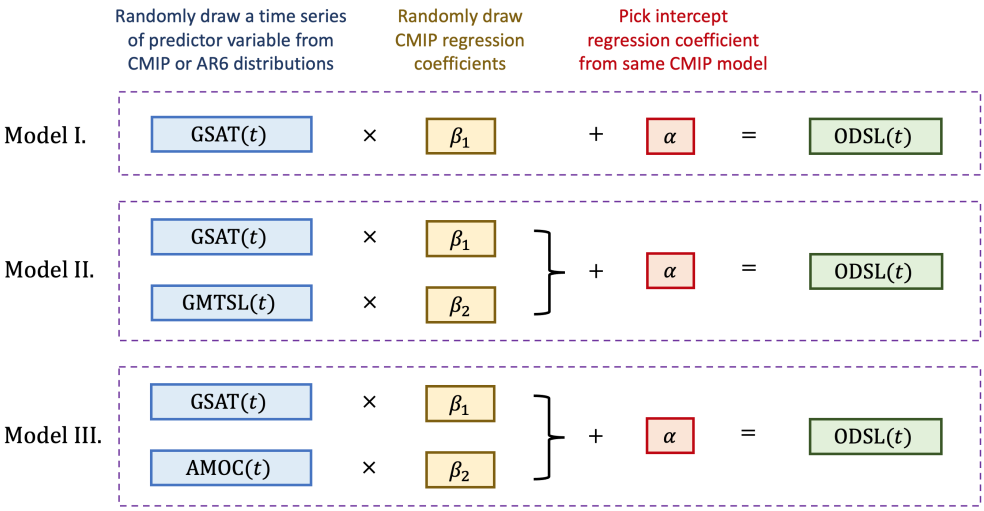

Figure 3.2: A schematic representation of the Monte Carlo simulation performed for the ODSL projections. The above process is repeated 10.000 times for both the CMIP ensemble, and the AR6 ensemble.

A schematic representation of the Monte Carlo simulation performed to construct the ODSL projections is shown in Figure 3.2. The first step is to randomly draw a time series for the predictor variables for a specific scenario. These time series are sampled from distributions that are constructed based on CMIP output for the CMIP ensemble, and on observations and AR6 ranges for the AR6 ensemble, shown in Figure 2.1. For the CMIP ensemble, we obtain the distributions by fitting a normal distribution to the CMIP output. Fitting a more complicated distribution raised problems due to the spread between models. For the AR6 ensemble, we fitted a Weibull distribution to the observations and AR6 ranges because these were slightly skewed. We did not fit any distribution for the observations from 1960 - 2005 because the uncertainty is negligible for that period. Note that there are no observations or AR6 assessed ranges for AMOC. Therefore, the AR6 ensembles using Model III also use the CMIP output of AMOC to create the sampling distributions. The time series is then created by randomly selecting an index of the sorted distribution and using this same index for every time step. That way, we follow a certain percentile of the distribution and obtain a smooth time series for the input variables. For the multiple models (II and III), we do not assume any relation between the predictor variables. This means that we randomly select the index for each predictor variable separately.

The second step is to randomly draw the regression coefficients computed in the regression analysis from either CMIP5 or CMIP6. These are then combined with the time series of the predictor variable. The corresponding offset α is added to these results, and with that, one time series of ODSL is constructed.

This process is repeated 10.000 times for all three emission scenarios for both the CMIP and AR6 ensemble and both the CMIP5 and CMIP6 regression coefficients. This thus results in 12 ensembles of ODSL projections. For each scenario and both CMIP5 and CMIP6, we can compute the difference between the CMIP ensemble and the AR6 ensemble. This can be used as a correction factor for the difference in GSAT and possibly GMTSL between the CMIP projections and assessed AR6 ranges. This correction factor can then be

subtracted from the original ODSL projections to obtain projections that are consistent with the AR6 ranges. By analysing the resulting corrected projections from CMIP5 and CMIP6, we can see if the temperature difference explains the difference in ODSL.

4 Results

4.1 Regression Analysis

In this section, we show the results of the different regression models used to get more insights into the drivers of ODSL change along the Dutch coast. We will first discuss the overall performance of the different regression models based on the metric RMSE. Then, we will discuss each model in detail where we also focus on the difference between the sensitivity to the predictor variables in CMIP5 and CMIP6.

4.1.1 Performance of Regression Models

Table 4.1 shows an overview of the CMIP5 and CMIP6 ensemble average RMSE for the different regression models. The smaller the RMSE, the more the predicted values are in line with the real data. Using an additional predictor variable lowers the RMSE values for both CMIP5 and CMIP6. For CMIP5, we see that both additional predictor variables have the same effect on the RMSE, whereas for CMIP6, including the AMOC leads to a lower RMSE than using GMTSL. The RMSE values thus suggest that the multiple linear model using AMOC and GSAT as predictors performs best for CMIP6. Note that for CMIP5, we find a smaller RMSE for each of the regression models compared to CMIP6. The difference in RMSE score is most pronounced in the linear GSAT model. The RMSE scores for the individual models can be found in Appendix C.

	Model I **GSAT**		Model II **GSAT + GMTSL**		Model III **GSAT + AMOC**	
	CMIP5	CMIP6	CMIP5	CMIP6	CMIP5	CMIP6
# of models	27	31	23	20	9	15
RMSE [cm]	3.10	10.19	2.36	6.25	2.36	4.54

Table 4.1: Regression results for the CMIP data for different regression models. The regression is performed on concatenated time series from the available CMIP models. The number of models available for each model is listed in the table.

These metrics give a quick overview of the performance of the different models. It is, however, also important to analyse how the regression models perform for the different scenarios. Furthermore, it is interesting to study the relative importance of the different predictors in the multiple linear models and see if that changes between CMIP5 and CMIP6. We will discuss each regression model separately in the coming subsections to further investigate this.

4.1.2 Model I: GSAT as Predictor

Figure 4.1 shows the time series of the ensemble-averaged regression model and the different terms for Model I using GSAT as a predictor variable. For CMIP5, the simple linear regression model is able to predict ODSL changes for the historic period and the different scenarios. For CMIP6, however, the regression model overestimates ODSL between 1960 - 2010. Thus, it cannot capture the drop in 1960 projected by the CMIP6 models. Furthermore, the ODSL change is underestimated at the end of the 21st century for both the lower (SSP1-2.6) and intermediate (SSP2-4.5) scenarios. For the higher (SSP5-8.5) emission scenario, we find that the regression model overestimates the ODSL change at the end of the century. Here, the ODSL rise projected by the CMIP6 models is nearly linear, whereas the regression model projects an exponential increase in ODSL.

Figure 4.2 shows a frequency histogram of the values for regression coefficient β_1. This visualisation allows us to analyse the scaling of GSAT and ODSL and the difference between CMIP5 and CMIP6. We mostly find positive values for β_1, indicating a positive correlation between GSAT and ODSL. For most models, both in CMIP5 and CMIP6, an increase of GSAT thus relates to a rise of ODSL along the Dutch coast. For CMIP5, we find an average β_1 of 3.62 cm/K. This means that, on average, with every GSAT increase of one degree,

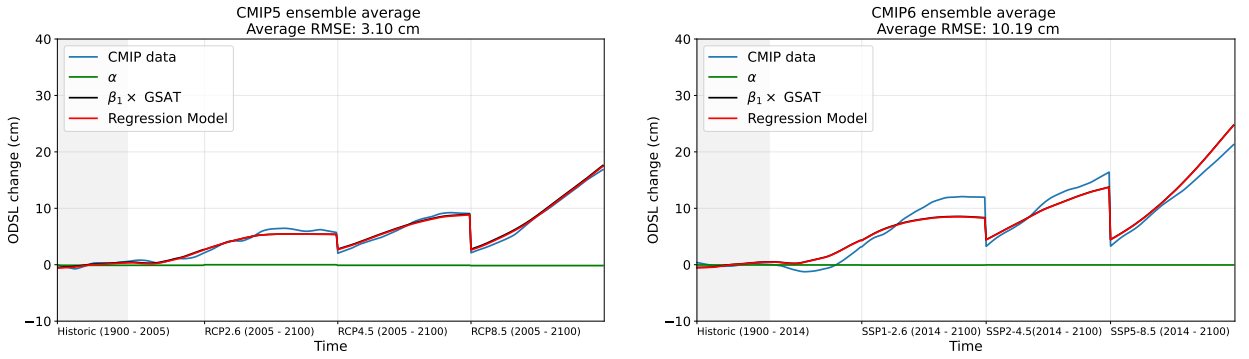

(a) CMIP5 (b) CMIP6

Figure 4.1: Ensemble-averaged regression for CMIP5 (a) and CMIP6 (b) based on Model I. The average RMSE is shown in the title. The x-axis covers the historical run, and three scenario runs for low, intermediate and high emissions. The different colours denote the ensemble average CMIP ODSL data (blue), the contributing terms of the regression model (green, black) and the total regression model (red). The reference period 1900 - 1949 is marked by grey shading.

ODSL rises by 3.62 cm for the CMIP5 models. Note that six CMIP5 models show a value of β_1 close to zero. The individual model plots (see Appendix C) show that these models are also the ones that project nearly no change in ODSL. For CMIP6, we find that both the average and the spread of β_1 are larger than in the CMIP5 models. However, we must keep in mind that the regression model does not perform well for the CMIP6 ensemble, so we should be careful analysing this set of regression parameters.

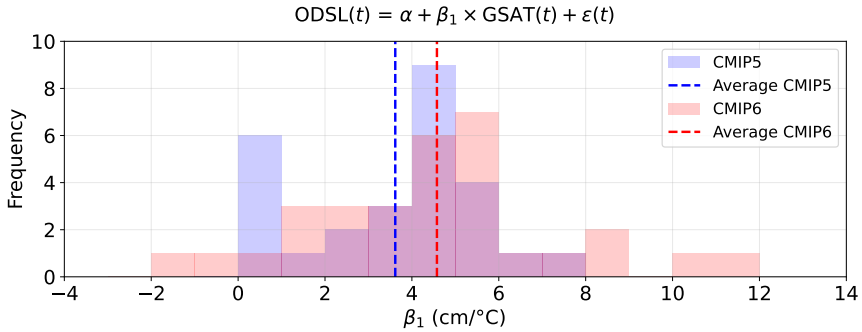

Figure 4.2: Frequency histogram plot of β_1 values for Model I using GSAT as a regressor. Blue colors indicate CMIP5 values and red indicate CMIP6 values. The dashed lines indicate the average β_1.

Generally, we thus find a positive correlation between GSAT and ODSL along the Dutch coast. Furthermore, we find that this regression model is able to capture most of the long-term variability of ODSL in CMIP5. For CMIP6 however, this is not the case. This motivates us to investigate the other predictor variables.

4.1.3 Model II GSAT and GMTSL as Predictors

Figure 4.3 shows the ensemble-averaged results of the regression analysis using Model II, which includes GMTSL as an additional predictor variable. The different colours again denote the different contributors to the total regression model. Model II is able to capture most long term changes in ODSL for the CMIP5 ensemble. The flattening of the ODSL rise in the lower emission scenario is captured, and the average RMSE is fairly low. For the higher emission scenario, the model slightly overestimates the end of the century ODSL. In the last half of the century, the regression model somewhat overestimates the trend. The contributions

from GSAT and GMTSL are almost equal for all scenarios. The contribution from the GSAT component is more critical at the beginning of the scenario runs, but at the end of the century both processes contribute equally. For CMIP6, not all long-term changes can be predicted by Model II. Again, the drop in 1960 is not captured by the regression model. Furthermore, ODSL is underestimated from 2040 - 2080 in both the lower and intermediate scenarios. For the higher emission scenario, the regression model overestimates the end of the century ODSL change by more than 5 cm. Also, the regression model trend at the start of the 21st century is smaller than the trend in the CMIP6 projections. The figure also indicates that the contribution from GMTSL became relatively more important in CMIP6 models. However, there is not a big difference between the CMIP5 and CMIP6 GMTSL projections (Appendix A). Therefore, the larger contribution of GMTSL in CMIP6 must be due to a larger dependence on the variable, and thus larger values for β_2, in the regression model.

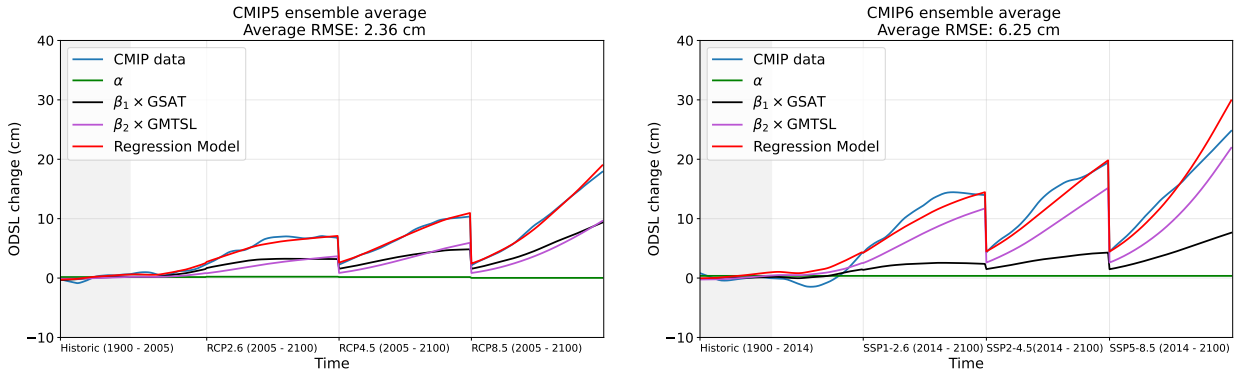

(a) (b)

Figure 4.3: Ensemble-averaged regression for CMIP5 (a) and CMIP6 (b) based on Model II. The average RMSE is shown in the title. The x-axis covers the historical run, and three scenario runs for low, intermediate and high emissions. The different colours denote the ensemble average CMIP ODSL data (blue), the contributing terms of the regression model (green, black) and the total regression model (red). The reference period 1900 - 1949 is marked by grey shading.

To investigate the latter, we visualise the regression coefficients of Model II in Figure 4.4. For CMIP6, the average dependence on GSAT is smaller, and the spread in β_1 is larger (left panel). For several models, a negative value for β_1 is obtained, indicating a negative relation between GSAT and ODSL. The scatter plot shows that those models have a larger dependence on GMTSL. For most models, however, a positive value for β_1 is found, indicating a positive relation, just as was found for Model I. Looking at the right panel, we see that the GMTSL dependence on average doubled in the CMIP6 models compared to the CMIP5 models. Also, we see a larger spread for the CMIP6 models. Most models show a positive relation between ODSL and GMTSL. However, some models, especially in CMIP5, show a negative relation. The on average lower β_1, and larger β_2 in CMIP6 explains the difference in the ratio of the contributors between CMIP5 and CMIP6 that we see in Figure 4.3. The negative values for the regression coefficients show that we must be careful with giving physical meaning to the coefficients. We are aware of this, and it is further discussed in Section 5.

From the presented results, we conclude that the regression model performs well for the CMIP5 ensembles. For CMIP6, however, the model performs less well. Especially the drop in the historic period and the overestimation of the higher emission scenario are remarkable. Nonetheless, we see that including GMTSL reduces the RMSE and improves the projections for the end of the 21st-century projections in the lower and intermediate emission scenario. Additionally, we find that the relative importance of the different predictor variables changes between CMIP5 and CMIP6.

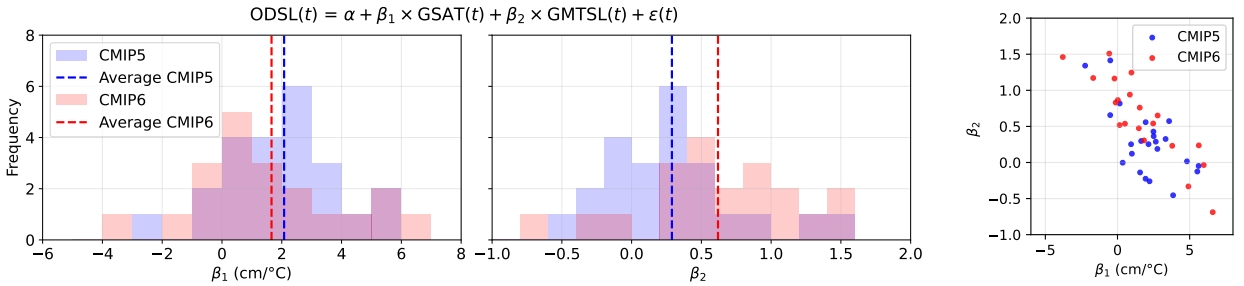

(a) (b)

Figure 4.4: Frequency histogram (a), and scatter plot (b) of β_1 and β_2 values for Model II, which uses GSAT and GMTSL as regressors. Blue colors indicate CMIP5 values and red indicate CMIP6 values. The dashed lines in (a) indicate the ensemble average values for the regression coefficients.

4.1.4 Model III: GSAT and AMOC as Predictors

Our third model includes the strength of the AMOC as an additional predictor variable besides GSAT. The results of the regression analysis using Model III are shown in Figure 4.5. For CMIP5, the regression model is able to predict the end of the century ODSL change well. However, the regression model does not capture the enhanced ODSL level between 2040 and 2070 in the lower emission scenario RCP2.6. Furthermore, we see that the contribution of the AMOC (yellow) is rather low with respect to the contribution of GSAT (black). For CMIP6, we see that Model III is able to capture most of the long-term variability in ODSL. The model also captures the drop of ODSL in 1960, whereas Model I and II were unable to do so. Furthermore, we see that it captures the flattening of ODSL at the end of the century in the lower emission scenario. For the higher emission scenario, we see that the regression model does a good job at predicting the ODSL change at the end of the century, whereas Model I and II overestimated it. One remarkable difference between the two ensembles is that the contribution from the AMOC term is substantially larger in CMIP6.

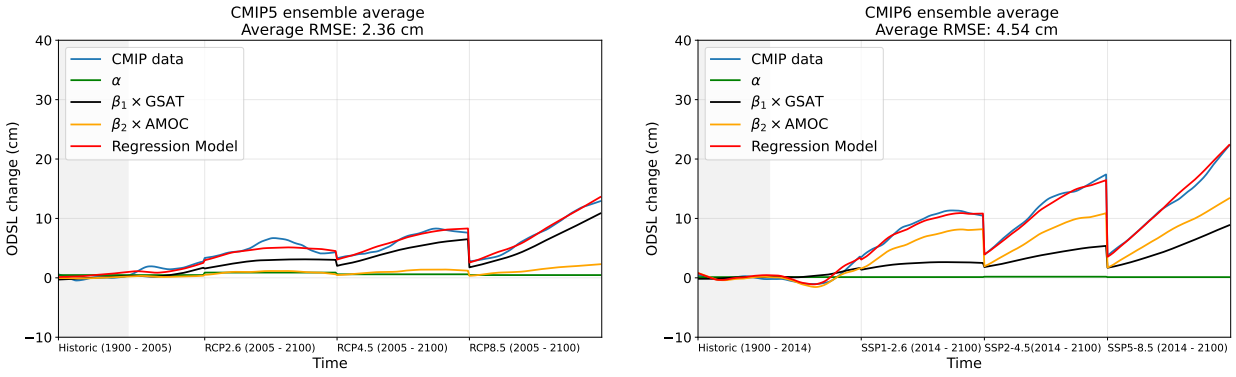

(a) CMIP5 (b) CMIP6

Figure 4.5: Ensemble-averaged regression for CMIP5 (a) and CMIP6 (b) based on Model III. The average RMSE is shown in the title. The x-axis covers the historical run, and three scenario runs for low, intermediate and high emissions. The different colours denote the ensemble average CMIP ODSL data (blue), the contributing terms of the regression model (green, black) and the total regression model (red). The reference period 1900 - 1949 is marked by grey shading.

This difference between CMIP5 and CMIP6 is also clear from the distributions of the regression coefficients, plotted in Figure 4.6. Again, we see that the dependence on GSAT is primarily positive, and a slightly smaller average β_1 is found for CMIP6. For the AMOC dependence, most models show a negative value

for β_2 and thus a negative relation. From the scatter plot, we see that models with a larger dependence on GSAT show a lower dependence on AMOC. The physical interpretation is further discussed in Section 5. For CMIP6, we see that the average β_2 is three times more negative than the average β_2 from CMIP5, thereby indicating that the dependence on AMOC increased between CMIP5 and CMIP6. Furthermore, the spread in β_2 is large in CMIP6 compared to CMIP5. For β_1 it is the other way around.

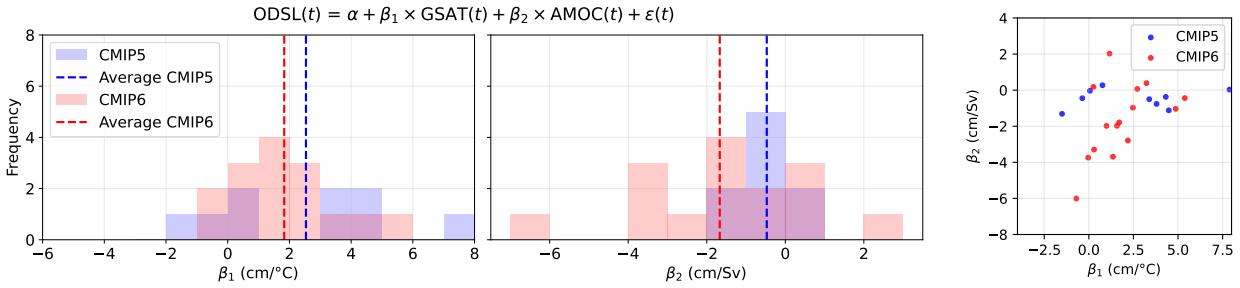

(a) (b)

Figure 4.6: Frequency histogram (a), and scatter plot (b) of β_1 and β_2 values for Model III, which uses GSAT and AMOC as regressors. Blue colors indicate CMIP5 values and red indicate CMIP6 values. The dashed lines in (a) indicate the ensemble average values for the regression coefficients.

To summarise, we find that including AMOC as an additional predictor variable improves the predictive power, especially for CMIP6. Most models show a negative relation between AMOC strength and ODSL along the Dutch coast. This relation is stronger in CMIP6, and therefore the relative contribution of the AMOC is larger. Here, it is important to keep in mind that only 9 models for CMIP5 and 15 models for CMIP6 were used for the analysis.

4.2 Probabilistic ODSL Ensembles and Corrections

This section contains the results for the ODSL reconstructions based on the regression analysis. We choose to reconstruct ODSL based on Model II and Model III. The results for these models are separately discussed in the following sections. We do not reconstruct ODSL based on Model I because this model is not suited for CMIP6.

4.2.1 Ensembles based on Model II

The motivation to use Model II to reconstruct ODSL is twofold. First, the regression model is based on a sufficient number of models and it is able to predict end-of-the-century ODSL change reasonably well for both ensembles, except for the higher emission scenario in CMIP6. Second, the AR6 provides ranges for both predictor variables GSAT and GMTSL. Therefore, we can correct for both variables and construct projections that are consistent with both ranges.

Figure 4.7 shows the time series of the median reconstructed ODSL using the CMIP input (purple) and the AR6 input (green) for all scenarios for both CMIP5 and CMIP6. The black dashed line shows the median of the original CMIP data for that specific scenario. Note that the CMIP ensemble projects a different change than the original data. This is partly due to the regression model not being able to capture the ODSL change exactly, and partly because the normal distributions that we use as input differ slightly from the CMIP output. We thus focus on the difference between the CMIP ensemble and the AR6 ensemble since it is difficult to compare the AR6 ensemble with the original CMIP data. Focusing on CMIP5, we see that correcting for

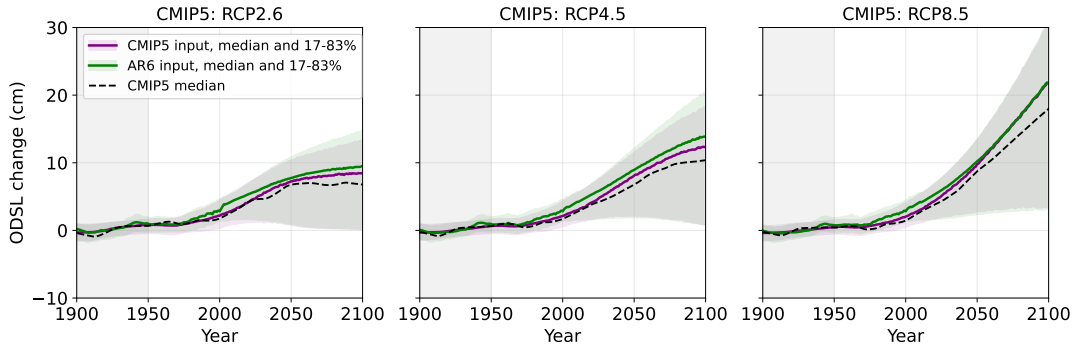

(a) CMIP5

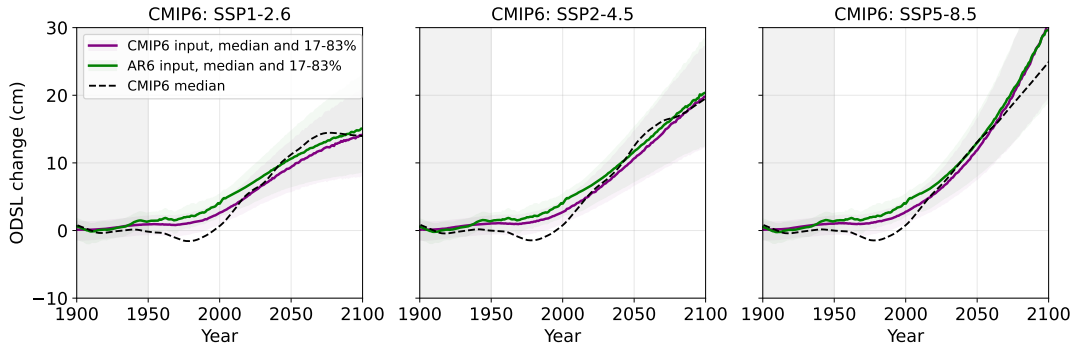

(b) CMIP6

Figure 4.7: Time series of the CMIP ensemble (purple) and the AR6 ensemble (green) based on Model II. Results are shown for both CMIP5 and CMIP6, for different scenarios. The median and 17 - 83 percentile are shown. The black dashed line represents the median of the CMIP models.

GSAT and GMTSL results in a slightly larger ODSL change in the 21st century for the lower and intermediate emission scenarios. For the higher emission scenario, we see that the AR6 model input first increases

the ODSL projections from 1970 - 2030, but at the end of the century, the difference is practically zero. For CMIP6, the AR6 input also increases the ODSL projections for the lower emission scenario. Furthermore, the ODSL projections based on AR6 input are larger than those based on CMIP in the period 1950 - 2020 for the intermediate and higher emission as well.

The difference between the green and purple lines from Figure 4.7 is plotted in Figure 4.8. This difference, as mentioned in Section 3, can be interpreted as a correction factor for the original ODSL data. For CMIP5, the difference between the two probabilistic ensembles is around zero during the 20th century and up until 2050. From 2050 on, the difference increases for the lower and intermediate emission scenarios. However, the difference is very small compared to the total ODSL change. For CMIP6, we see that the difference between the CMIP ensemble and the AR6 ensemble is around 1 cm for all scenarios from 1950 - 2050. After that, the difference decreases for the lower and intermediate emission scenarios. For the higher emission scenario, the difference decreases as well but then increases to the opposite sign after 2080.

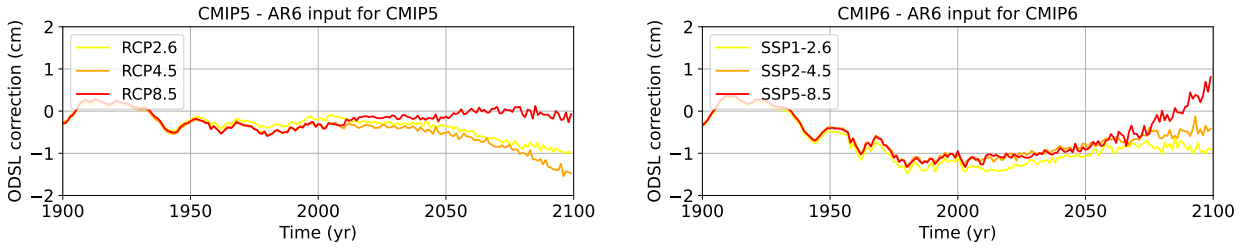

(a) CMIP5 (b) CMIP6

Figure 4.8: The difference between the CMIP emsemble and AR6 ensemble for different scenarios based on Model II.

We can also visualise the end of the century projections from both ensembles. Figure 4.9 shows the percentiles for the average ODSL change over the years 2081 - 2100. The purple bars indicate the results for the CMIP ensemble, and the green bars indicate the results for the AR6 ensemble. At first sight, not much difference is seen between the two probabilistic ensembles. For both ensembles, the spread increases slightly in the AR6 ensemble. If we look in detail, we see that the median decreases slightly for all scenarios in CMIP6 when using the AR6 assessed ranges. For CMIP5, the AR6 input increases the median for the lower and intermediate emission scenarios and decreases the median for the higher emission scenario. Furthermore, we see that for CMIP5, the lower end of the uncertainty is larger than the upper end. This is also obvious from

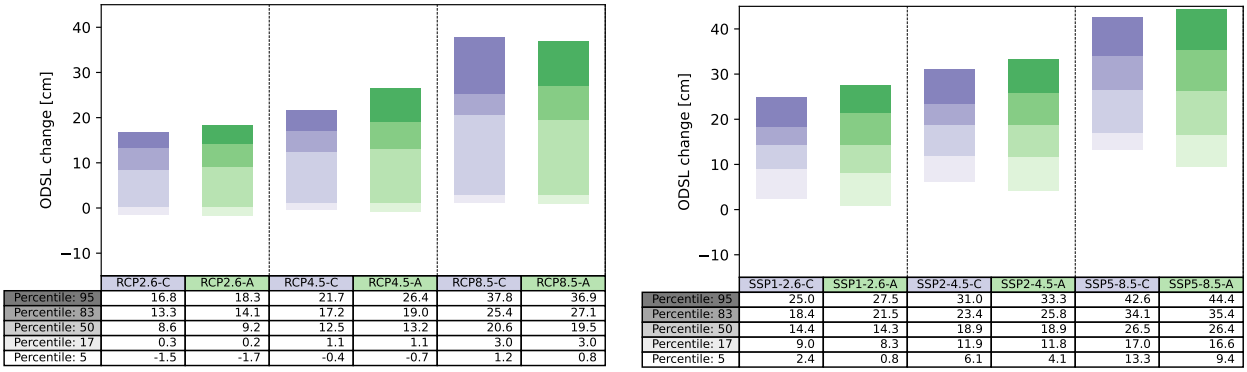

	RCP2.6-C	RCP2.6-A	RCP4.5-C	RCP4.5-A	RCP8.5-C	RCP8.5-A
Percentile: 95	16.8	18.3	21.7	26.4	37.8	36.9
Percentile: 83	13.3	14.1	17.2	19.0	25.4	27.1
Percentile: 50	8.6	9.2	12.5	13.2	20.6	19.5
Percentile: 17	0.3	0.2	1.1	1.1	3.0	3.0
Percentile: 5	-1.5	-1.7	-0.4	-0.7	1.2	0.8

(a) CMIP5

	SSP1-2.6-C	SSP1-2.6-A	SSP2-4.5-C	SSP2-4.5-A	SSP5-8.5-C	SSP5-8.5-A
Percentile: 95	25.0	27.5	31.0	33.3	42.6	44.4
Percentile: 83	18.4	21.5	23.4	25.8	34.1	35.4
Percentile: 50	14.4	14.3	18.9	18.9	26.5	26.4
Percentile: 17	9.0	8.3	11.9	11.8	17.0	16.6
Percentile: 5	2.4	0.8	6.1	4.1	13.3	9.4

(b) CMIP6

Figure 4.9: Average ODSL change for the CMIP ensemble (purple) and the AR6 ensemble (green) for CMIP5 (a) and CMIP6 (b), computed using Model II.

Figure 4.7. Since the input distributions are either normally distributed (CMIP ensemble) or only slightly skewed (AR ensemble), this larger uncertainty at the low end has to be the result of the model parameters. Some models show only slight or no changes in ODSL and therefore have values around zero for both β_1, and β_2 (see Appendix C), which results in the low projections in the ensembles. This result agrees with Figure 1.4, where we also see that the low-end uncertainty is larger for the original CMIP5 data.
In summary, the correction using AR6 assessed ranges for GSAT and GMTSL is very small. In the regression analysis, we found that most models show a positive relation between ODSL and both these variables. Since the AR6 GSAT ranges are higher (lower) than CMIP5 (CMIP6) GSAT, we would expect an increase (decrease) of ODSL due to that correction (see Appendix A). For GMTSL however, the AR6 assessed ranges are slightly higher than the CMIP5 and CMIP6 projections of GMTSL. The correction for this component would thus lead to a decrease in ODSL. These two terms then cancel each other out and lead to nearly no difference between the CMIP and AR6 ensembles.

4.2.2 Ensembles based on Model III

Using Model III as a basis for our reconstruction has, again, a twofold motivation. First, this regression model performed well for both ensembles and is able to capture the drop in ODSL in CMIP6. Second, it is of value to include this local process in the projections because previous work shows the importance of AMOC for ODSL in several nearby regions (Katsman et al., 2008; Lyu et al., 2020). The downside of using Model III is that fewer CMIP models have data available for the predictor variables, whereas we would like to base our reconstructions on as many models as possible. On top of that, the CMIP6 members that do provide data for these variables do not show a big difference between their GSAT projections and the assessed AR6 ranges. Therefore, the correction for temperature would not lead to a difference in ODSL and, besides, does

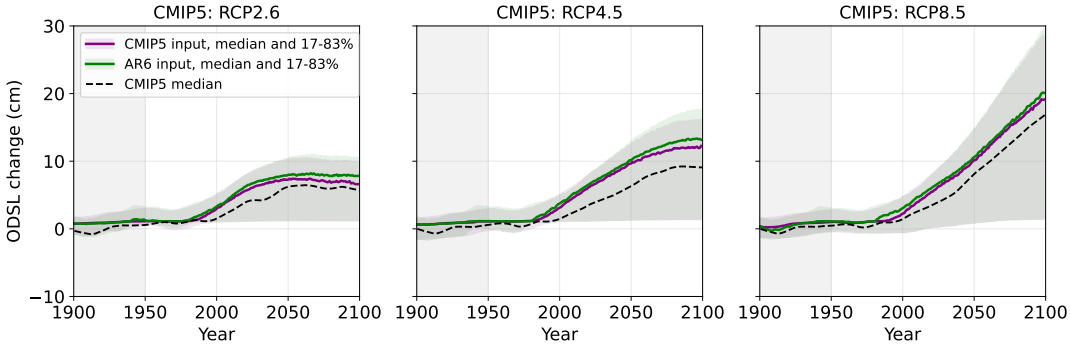

(a) CMIP5

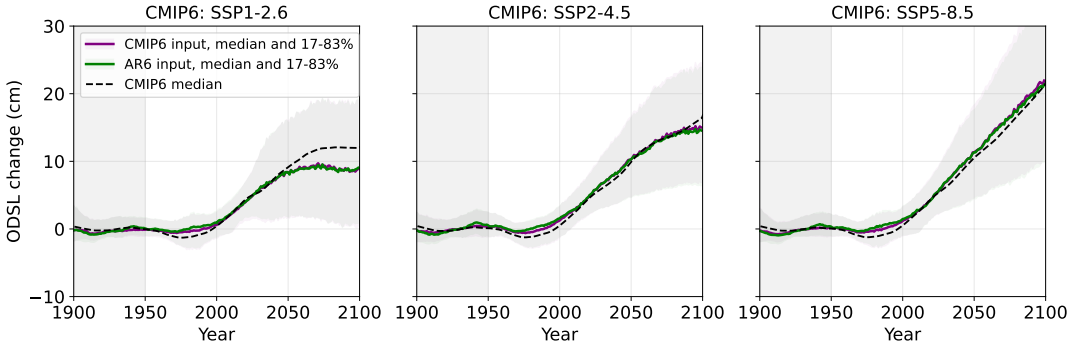

(b) CMIP6

Figure 4.10: Time series of the CMIP ensemble (purple) and the AR6 ensemble (green) based on Model III. Results are shown for both CMIP5 and CMIP6, for different scenarios. The median and 17 - 83 percentile are shown. The black dashed line represents the median of the CMIP models.

not really have a purpose. In order to be able to use Model III for the ODSL correction, we propose the following solution. Instead of using only the CMIP output from models that have ODSL, GSAT, and AMOC available, we also use the GSAT output from models that have data available for only ODSL and GSAT to compute the distributions. Thereby, we assume that the relation between ODSL, GSAT, and AMOC also holds for the other models that have no AMOC data available. The resulting distributions are then used as the input for the Monte Carlo sampling method for the CMIP ensemble.

Figure 4.10 shows the time series of the medians from the probabilistic ensembles using this method. For CMIP5, the AR6 ensemble shows slightly more ODSL rise at the end of the century for the lower and intermediate emission scenarios. For the higher emission scenario, the difference between the two ensembles is very small. For CMIP6, the AR6 ensemble shows slightly less rise in ODSL for all three scenarios. Figure 4.11 visualises the differences between the ensembles more clear. For both ensembles, we see little difference in the historical period. For CMIP5, we see that the difference increases from 2050 on, especially for the intermediate emission scenario. For CMIP6, we see that the difference increases from 2000 on. The difference at the end of the century is largest (1 cm) for the higher emission scenario.

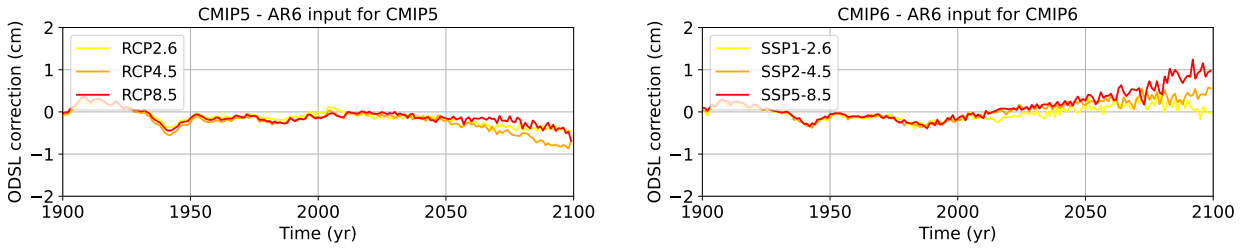

(a) CMIP5 (b) CMIP6

Figure 4.11: The difference between the CMIP emsemble and AR6 ensemble for different scenarios based on Model III.

From the above plots, we see that the most pronounced differences are at the end of the 21st century. Figure 4.12 compares the percentiles for the average end-of-the-century ODSL change from the CMIP and AR6 ensembles. Again, we see that the difference between the green and purple bars is small. This is due to the relatively low importance of the GSAT term in the regression model. Since we do not correct for AMOC, the correction is only minimal. The AR6 ensembles for CMIP5 show slightly more spread than the CMIP ensembles, but there is little difference between the medians. The latter is also the case for CMIP6. The

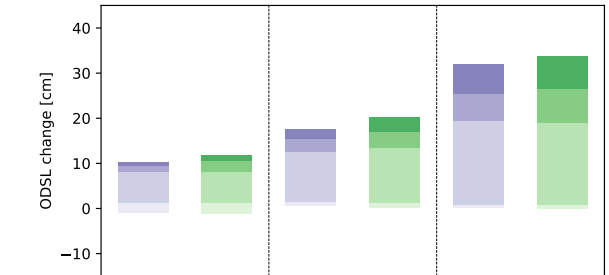

	RCP2.6-C	RCP2.6-A	RCP4.5-C	RCP4.5-A	RCP8.5-C	RCP8.5-A
Percentile: 95	10.3	11.8	17.4	20.3	32.1	33.7
Percentile: 83	9.5	10.5	15.4	17.1	25.5	26.6
Percentile: 50	8.1	8.2	12.7	13.4	19.5	19.0
Percentile: 17	1.3	1.3	1.4	1.4	0.8	0.9
Percentile: 5	-1.0	-1.3	0.7	0.2	0.1	-0.1

(a) CMIP5

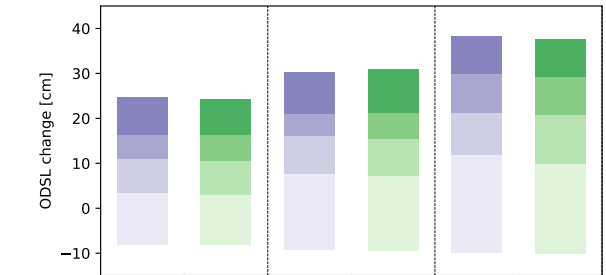

	SSP1-2.6-C	SSP1-2.6-A	SSP2-4.5-C	SSP2-4.5-A	SSP5-8.5-C	SSP5-8.5-A
Percentile: 95	24.7	24.3	30.4	30.8	38.3	37.7
Percentile: 83	16.4	16.5	21.1	21.2	30.0	29.3
Percentile: 50	10.9	10.6	16.1	15.5	21.3	20.7
Percentile: 17	3.5	2.9	7.7	7.3	11.9	9.8
Percentile: 5	-8.2	-8.2	-9.2	-9.4	-9.9	-10.1

(b) CMIP6

Figure 4.12: Average ODSL change for the CMIP ensemble (purple) and the AR6 ensemble (green) for CMIP5 (a) and CMIP6 (b), computed using Model III.

intermediate and higher emission scenarios show a 0.7 cm and 0.8 cm reduction, respectively. For the lower emission scenario, the results of the CMIP ensemble and the AR6 ensemble are very similar. This difference between the scenarios can be explained by the change in relative importance of the AMOC in the regression model in 4.5. For the lower emission scenario, the relative contribution of GSAT is smaller than for the intermediate and higher emission scenarios. Again, we see that the uncertainty's lower end is larger compared to the upper end. For CMIP6, the bar even extends to a decrease in ODSL at the end of the century. This is probably due to a few CMIP6 models having positive values for β_2, which then leads to a drop in ODSL when combined with a strong weakening of the AMOC.

To summarise, we find that the correction for the AR6 assessed temperatures based on Model III is small. This is partly due to the little importance of GSAT in the CMIP6 regression model, and partly due to the fact that we can not correct for the AMOC.

5 Discussion

5.1 Regression Analysis and Projections

In this study, we used linear regression to investigate different possible drivers of ODSL along the Dutch coast. Thus, we assumed a linear relation between ODSL and the predictor variables. This is in agreement with earlier pattern scaling studies (Bilbao et al., 2015; Palmer et al., 2018; Yuan and Kopp, 2021). More complicated regression models could also be considered. However, we found that a quadratic dependence of ODSL on GSAT did not improve the regression model. An advantage of using simple linear regression models is that it is easier to give physical meaning to the model, and it reduces the problem of overfitting. Additionally, they are computationally fast because of their simplicity.

The physical interpretation of Model I is more straightforward than the other models. For Model I, we can generally say that an increase in GSAT relates to an increase in ODSL. For Model II and III, however, we considered two predictor variables that are to some extent correlated with each other. This so-called 'multicollinearity' does not affect the predictive power of the regression model, but we do have to be careful with interpreting the results. For example, we know that an increase in GSAT leads to an increase in GMTSL via the process of thermal expansion, thus indicating a positive correlation between the two variables. Nonetheless, for Model II, we found some individual models with a negative dependence on GSAT and a positive dependence on GMTSL or the other way around. Hence, this does not make any physical sense and is just an effect of the optimisation of the linear regression model. For most models, however, we found a positive dependence on both GSAT and GMTSL. Still, we have to be careful with the interpretation of the results. Due to multicollinearity, the regression coefficients are sensitive to minor changes in the data. Therefore, we should be careful with interpreting the importance of the different variables. For both Model II and Model III, we saw that the relative importance of the additional predictor (GMTSL or AMOC) increased in the CMIP6 ensemble. For Model III however, we find that reducing the size of the smoothing window reduces the relative importance of the AMOC in the regression model (see Appendix D). This indicates that the short-term variability in ODSL seems to be influenced more by GSAT, and the longer-term variability by the AMOC. We are aware that the sensitivity of the relative importance of the different variables also influences the probabilistic ensembles because these are based on the regression coefficients. If these would slightly change, the correction would also depend more or less on either of the variables. Nonetheless, we choose to base our reconstructions on the multiple linear models Model II and Model III, because Model I, which only includes GSAT, does not perform well for CMIP6. Also, Model II enables us to make the ODSL projections consistent with both AR6 assessed ranges for GSAT and GMTSL.

The regression analysis showed that Model III performed best at predicting ODSL for both ensembles. However, we should keep in mind that these results are based on relatively few models (9 for CMIP5, and 15 for CMIP6) due to the limited availability of AMOC data. Since some of these models are developed by the same modeling group, this is a problem for the robustness of our conclusion. To check the robustness of Model III, we would like to include more data from different models. Including more models would also improve the probabilistic ensembles based on this regression model. Then we can compute the relation between ODSL, GSAT, and AMOC for each model, instead of assuming that the same relation holds for other models currently not providing the AMOC data. Another comment on the regression analysis is that we did not measure the uncertainties in the coefficients. Different methods to include this are discussed in Jevrejeva et al., 2019. For instance, a bootstrapping method could be used to compare the CMIP5 and CMIP6 sensitivity. This would make the conclusions on the difference between CMIP5 and CMIP6 more robust.

Lastly, reflecting on the correction method, we can make two remarks. First, an assumption is made in the construction of the distributions by fitting normal distributions to the CMIP data even though the data is not necessarily normally distributed, especially not for GMTSL and AMOC (Appendix A). Fitting more complex distributions to the CMIP data led to substantial overestimation of the skewness and did not give proper results. The normal distribution is thus the best approximation and it is also in agreement with AR5, where they fit normal distributions to GSAT data from the CMIP models to obtain the projected ranges. A second remark on the correction method is that we only have assessed ranges of GSAT and GMTSL,

and not of AMOC. For Model III, we thus only correct for GSAT and use the CMIP output for AMOC for both the CMIP and AR6 ensemble. However, these distributions have a large spread and this uncertainty then propagates to the probabilistic ensembles. Constraining the input of the AMOC could lead to lower uncertainty in the reconstructions, and a more accurate correction factor.

5.2 Mixed Layer Depth

The aim of the correction method was to make the ODSL projections from CMIP5 and CMIP6 consistent with the AR6 ranges. However, the correction factors that we find for both Model II and Model III are very small; therefore, the difference between the two ensembles remains. This raises the question what other processes could influence ODSL along the Dutch coast, and whether these processes change between CMIP5 and CMIP6.

One factor that could possibly influence local sea level is the location of deep convection. In this process, layers of water are mixed by mesoscale ocean circulation and strong winds. It plays an important role in the formation of bottom and intermediate water, and in the large-scale thermohaline circulation (Killworth, 1983). To investigate whether the location of open ocean convection influences ODSL along the Dutch coast, we analyse the mixed layer depth (MLD) data for the historic period from different models.

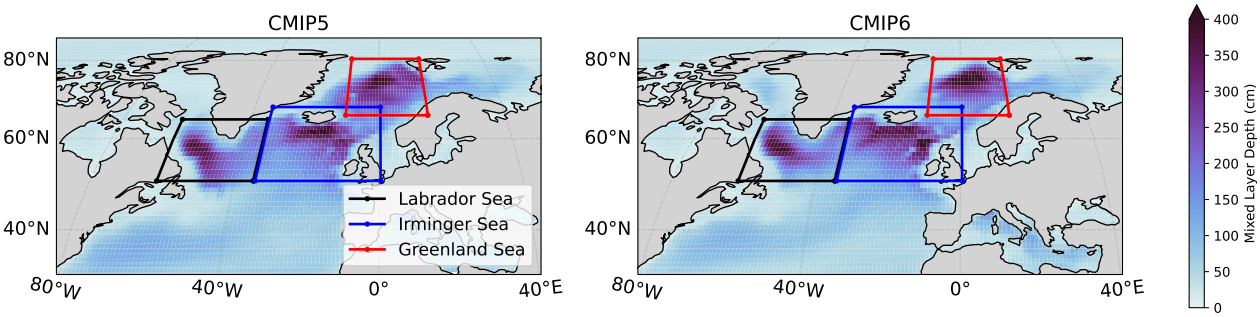

Figure 5.1: Multi-model mean mixed layer depth (MLD) computed as the average over 1975 - 2004. Three regions showing large values of MLD are indicated by the boxes.

Figure 5.1 shows the 1975 - 2004 ensemble mean MLD in the CMIP5 and CMIP6 models. The MLD for individual models can be found in Appendix E. The general pattern is similar for CMIP5 and CMIP6. Three regions are characterised by large values for the MLD: the Labrador Sea (black), the Irminger Sea (blue), and the Greenland Sea (red). The individual models are categorised based on in which of these regions their maximum MLD exceeds the threshold of 170 m. The models are then labelled with LS (Labrador Sea), IS (Irminger Sea), or GS (Greenland Sea). We allow the models to have multiple labels if they exceed the threshold for more than one region. By categorising the models, we can compare the ODSL projections from models showing deep convection in different regions. An interesting result is shown in Figure 5.2, where we compare the ODSL time series of the GS models with that of models that are not labelled with GS, so not showing a deep mixed layer. For all scenarios, and for both CMIP5 and CMIP6, we see that the GS models predict larger ODSL change than the other models. Looking at the end of the century, we see that the difference between the means of the two groups is around 10 cm for CMIP6, no matter the scenario. For CMIP5, the difference increases from around 4 cm for the lower emission scenario to 15 cm for the higher emission scenario. However, we must be careful with interpreting the CMIP5 results since only 8 to 10 models are included in this analysis due to the limited availability of MLD data. For CMIP6, more than half of the models exceed the threshold. For CMIP5, this fraction is smaller, although we must be careful with the limited amount of models.

These results suggest that the location of deep convection, characterised by a deep mixed layer, influences ODSL along the Dutch coast. More specifically, we find that models showing a deep mixed layer in the Greenland Sea during the period 1975 - 2004 project a larger rise of ODSL than other models. Since the difference between the GS models and the others is substantially large, it would be interesting to explore

this further. If more models in CMIP6 show a deep mixed layer in the Greenland Sea, this might also explain part of the difference between CMIP5 and CMIP6. However, we would have to obtain data for more CMIP5 models to make this statement conclusive. Furthermore, the location of deep convection might be used to constrain ODSL projections by only selecting models that show enhanced MLD at locations that agree with observations. Finally, it is important to point out that several studies find that MLD is overestimated in global climate models from CMIP5 and CMIP6 (Heuzé, 2021; Sohail et al., 2020). It will be interesting to further investigate whether this also leads to an overestimation of ODSL.

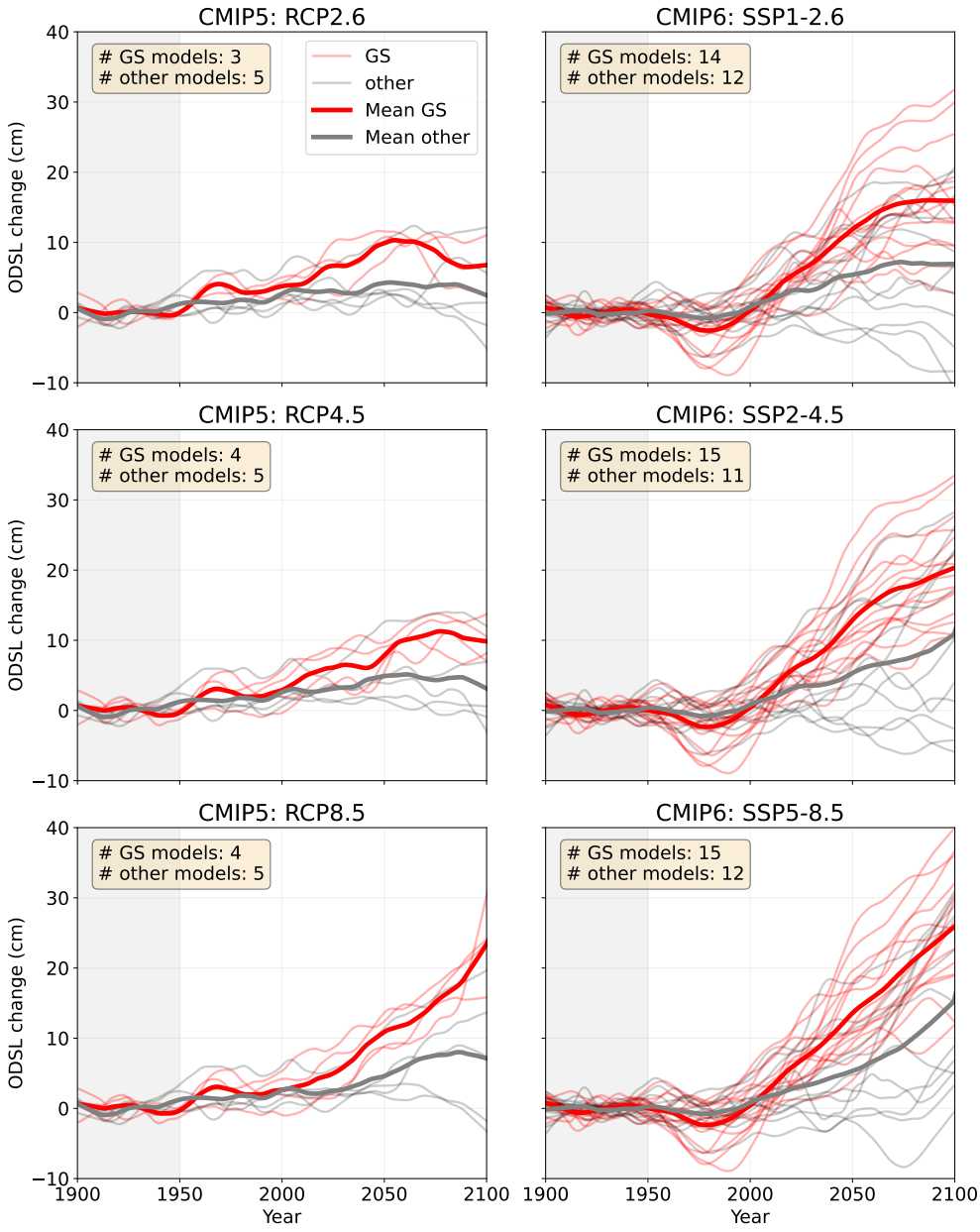

Figure 5.2: ODSL time series for two groups of models: GS models (red) and other models (grey). For the GS models, the maximum MLD in the Greenland Sea exceeds 170 m, whereas the maximum MLD in that same region is 170 m or shallower for the other models. The thin lines represent the time series of the individual models. The thick lines represent the mean of the two groups. The reference period 1900 - 1949 is marked by grey shading.

6 Conclusions and Suggestions

6.1 Conclusions

Now that the results and discussion points have been presented, we can answer the research questions formulated in Section 1.

1. *What processes can be related to ocean dynamic sea level change along the Dutch coast?*
   We found that most individual models from CMIP5 and CMIP6 show a positive correlation between GSAT and ODSL along the Dutch coast. For the CMIP5 ensemble, the linear scaling with GSAT enables us to predict the long-term variations in ODSL well. For CMIP6, however, we found that the regression model does not capture all variations in ODSL. This motivated us to look into other processes as well. The predictive power of the regression model improved by including GMTSL as an additional predictor, although it was still not able to capture all long-term changes in CMIP6. We found that most individual models show a positive relation between GMTSL and ODSL. For our third model, we included AMOC as an additional predictor variable besides GSAT. This model performed well for both ensembles. It captures the drop in ODSL between 1960 and 2000 seen in the CMIP6 ensemble, while the other regression models could not do so. Generally, we find a negative relation between AMOC and ODSL, indicating that a weakening of the AMOC is related to a rise of ODSL along the Dutch coast. Finally, we find that the location of deep convection is important for the ODSL projections along the Dutch coast. Models that show a deep mixed layer in the Greenland Sea for the period 1980 - 2000 project larger rise in ODSL along the Dutch coast than other models.
2. *Can the difference in predicted temperature increase between CMIP5 and CMIP6 models explain the difference in ocean dynamic sea level change?*
   Based on the method proposed in this work, the effect of GSAT is too small to explain the difference in ODSL between CMIP5 and CMIP6. Interestingly, Model II and Model III both point to the increased sensitivity of ODSL to processes in the ocean in CMIP6. This difference between the importance of the predictor variables in CMIP5 and CMIP6 is remarkable and might point to different model dynamics.
3. *Can we provide ocean dynamic sea level projections that are consistent with the AR6 assessed ranges of temperature and global mean thermosteric sea level?*
   We used the results from the multiple linear regression models to generate probabilistic ensembles either consistent with CMIP output of the predictor variables (CMIP ensemble), or with AR6 assessed ranges (AR6 ensemble). By subtracting the two ensembles, we found a correction factor which could then be subtracted from the original ODSL time series to obtain projections that are consistent with the AR6 assessed ranges of GSAT and, in the case of Model II, also GMTSL. Our results show that the correction is very small. On the one side, this can be attributed to the relatively little importance of GSAT in the regression models. On the other side, it is due to the difference between GMTSL from the CMIP models and the assessed range being small, and no correction being performed for the AMOC. Given the small correction that we found, it might not be worth the trouble of using a much more complex method to construct projections consistent with the AR6.

6.2 Suggestions for Future Research

The analysis of Model III is based on a smaller ensemble due to the limited availability of AMOC data. For this model's robustness, obtaining AMOC data for more models would be useful. We could compute this using the velocity fields. Additionally, other processes could be further investigated. For instance, the influence of the location of deep convection on ODSL, as we commented on in Section 5.2, showed interesting results. Furthermore, it would be useful to investigate whether models with the same ocean component also show similar changes in ODSL. Also, the resolution of the different ocean models is different (Hewitt et al., 2022). It would be good to explore whether this resolution influences local scale ocean dynamics. Lastly, the focus of this study is primarily on the Dutch coast. Nonetheless, the framework of the method can easily be applied to other regions as well. It might be of interest to see whether the importance of the predictor variables is different for other regions.

Acknowledgements

This project would not have been possible without the support of many people. First and foremost, I would like to thank my primary supervisor Dr. Dewi Le Bars. Thank you for the interesting discussions, useful insights and your enthusiasm about the research topic, and science in general. I really appreciate the time you took for our weekly meetings, which gave me the energy to continue with the research. Also, I would like to thank Prof. dr. Sybren Drijfhout and Prof. dr. Huib de Swart for providing me with feedback and useful insights during the project.

Moreover, I am very fortunate to have been a part of the Sea Level Team of KNMI during this project. Thank you for making me feel welcome in the group, for the nice coffee breaks, and for the interesting discussions and feedback on my research. I hope to visit the weekly sea level meetings now and then during my PhD, and I am sure we will keep in touch.

Furthermore, I want to thank my family, Ken, friends, and other people I met at KNMI for supporting me throughout the process. A special thanks to Ken, Brechtje, and Philippe for providing me with feedback on my introduction and writing style. Lastly, thanks to my fellow master students, who made it a pleasure to study in our master room on the sixth floor.

References

Bilbao, R. A., J. M. Gregory, and N. Bouttes (2015). "Analysis of the regional pattern of sea level change due to ocean dynamics and density change for 1993–2099 in observations and CMIP5 AOGCMs". In: *Climate Dynamics* 45.9, pp. 2647–2666.

Bingham, R. and C. Hughes (2012). "Local diagnostics to estimate density-induced sea level variations over topography and along coastlines". In: *Journal of Geophysical Research: Oceans* 117.C1.

Bouttes, N. and J. M. Gregory (2014). "Attribution of the spatial pattern of CO2-forced sea level change to ocean surface flux changes". In: *Environmental Research Letters* 9.3, p. 034004.

Bouttes, N., J. M. Gregory, T Kuhlbrodt, and R. Smith (2014). "The drivers of projected North Atlantic sea level change". In: *Climate Dynamics* 43.5, pp. 1531–1544.

Chen, C., W. Liu, and G. Wang (2019). "Understanding the uncertainty in the 21st century dynamic sea level projections: The role of the AMOC". In: *Geophysical Research Letters* 46.1, pp. 210–217.

Couldrey, M. P., J. M. Gregory, F. Boeira Dias, P. Dobrohotoff, C. M. Domingues, O. Garuba, S. M. Griffies, H. Haak, A. Hu, M. Ishii, et al. (2021). "What causes the spread of model projections of ocean dynamic sea-level change in response to greenhouse gas forcing?" In: *Climate Dynamics* 56.1, pp. 155–187.

Cunningham, S. A., T. Kanzow, D. Rayner, M. O. Baringer, W. E. Johns, J. Marotzke, H. R. Longworth, E. M. Grant, J. J.-M. Hirschi, L. M. Beal, et al. (2007). "Temporal variability of the Atlantic meridional overturning circulation at 26.5 N". In: *Science* 317.5840, pp. 935–938.

Fox-Kemper, B., H. Hewitt, C. Xiao, G. Aalgeirsdóttir, S. Drijfhout, T. Edwards, N. Golledge, M. Hemer, R. Kopp, G. Krinner, A. Mix, D. Notz, S. Nowicki, I. Nurhati, L. Ruiz, J.-B. Sallée, A. Slangen, and Y. Yu (2021). *Ocean, Cryosphere and Sea Level Change. In Climate Change 2021: The Physical Science Basis. Contribution of Working Group I to the Sixth Assessment Report of the Intergovernmental Panel on Climate Change*. [Masson-Delmotte, V., P. Zhai, A. Pirani, S.L. Connors, C. Péan, S. Berger, N. Caud, Y. Chen, L. Goldfarb, M.I. Gomis, M. Huang, K. Leitzell, E. Lonnoy, J.B.R. Matthews, T.K. Maycock, T. Waterfield, O. Yelekçi, R. Yu, B. Zhou (eds.)] Cambridge University Press, Cambridge United Kingdom, and New York, NY, USA, pp. 1211–1362, doi:10.1017/9781009157896.011.

Frederikse, T., F. Landerer, L. Caron, S. Adhikari, D. Parkes, V. W. Humphrey, S. Dangendorf, P. Hogarth, L. Zanna, L. Cheng, et al. (2020b). "The causes of sea-level rise since 1900". In: *Nature* 584.7821, pp. 393–397.

Frederikse, T., R. Riva, M. Kleinherenbrink, Y. Wada, M. van den Broeke, and B. Marzeion (2016). "Closing the sea level budget on a regional scale: Trends and variability on the Northwestern European continental shelf". In: *Geophysical Research Letters* 43.20, pp. 10–864.

Gill, A. and P. Niller (1973). "The theory of the seasonal variability in the ocean". In: *Deep Sea Research and Oceanographic Abstracts*. Vol. 20. 2. Elsevier, pp. 141–177.

Good, S. A., M. J. Martin, and N. A. Rayner (2013). "EN4: Quality controlled ocean temperature and salinity profiles and monthly objective analyses with uncertainty estimates". In: *Journal of Geophysical Research: Oceans* 118.12, pp. 6704–6716.

Gregory, J. M., N. Bouttes, S. M. Griffies, H. Haak, W. J. Hurlin, J. Jungclaus, M. Kelley, W. G. Lee, J. Marshall, A. Romanou, et al. (2016). "The flux-anomaly-forced model intercomparison project (fafmip) contribution to CMIP6: Investigation of sea-level and ocean climate change in response to CO2 forcing". In: *Geoscientific Model Development* 9.11, pp. 3993–4017.

Gregory, J. M., S. M. Griffies, C. W. Hughes, J. A. Lowe, J. A. Church, I. Fukimori, N. Gomez, R. E. Kopp, F. Landerer, G. L. Cozannet, et al. (2019). "Concepts and terminology for sea level: Mean, variability and change, both local and global". In: *Surveys in Geophysics* 40.6, pp. 1251–1289.

Hausfather, Z., K. Marvel, G. A. Schmidt, J. W. Nielsen-Gammon, and M. Zelinka (2022). "Climate simulations: Recognize the 'hot model'problem". In: *Nature*, pp. 26–29.

Hermans, T. H., J. Tinker, M. D. Palmer, C. A. Katsman, B. L. Vermeersen, and A. Slangen (2020). "Improving sea-level projections on the Northwestern European shelf using dynamical downscaling". In: *Climate Dynamics* 54.3, pp. 1987–2011.

Heuzé, C. (2021). "Antarctic bottom water and North Atlantic deep water in cmip6 models". In: *Ocean Science* 17.1, pp. 59–90.

Hewitt, H., B. Fox-Kemper, B. Pearson, M. Roberts, and D. Klocke (2022). "The small scales of the ocean may hold the key to surprises". In: *Nature Climate Change* 12.6, pp. 496–499.

Hinkel, J., D. Lincke, A. T. Vafeidis, M. Perrette, R. J. Nicholls, R. S. Tol, B. Marzeion, X. Fettweis, C. Ionescu, and A. Levermann (2014). "Coastal flood damage and adaptation costs under 21st century sea-level rise". In: *Proceedings of the National Academy of Sciences* 111.9, pp. 3292–3297.

Hobbs, W., M. D. Palmer, and D. Monselesan (2016). "An energy conservation analysis of ocean drift in the CMIP5 global coupled models". In: *Journal of Climate* 29.5, pp. 1639–1653.

Jevrejeva, S, T Frederikse, R. Kopp, G. Le Cozannet, L. Jackson, and R. Van De Wal (2019). "Probabilistic sea level projections at the coast by 2100". In: *Surveys in geophysics* 40.6, pp. 1673–1696.

Katsman, C. A., W. Hazeleger, S. S. Drijfhout, G. J. van Oldenborgh, and G. Burgers (2008). "Climate scenarios of sea level rise for the northeast Atlantic Ocean: a study including the effects of ocean dynamics and gravity changes induced by ice melt". In: *Climatic Change* 91.3, pp. 351–374.

KNMI (2021). "KNMI Klimaatsignaal'21: hoe het klimaat in Nederland snel verandert." In: *KNMI, De Bilt,* 72 pp.

Lee, J.-Y., J. Marotzke, G. Bala, L. Cao, S. Corti, J. Dunne, F. Engelbrecht, E. Fischer, J. Fyfe, C. Jones, A. Maycock, J. Mutemi, O. Ndiaye, S. Panickal, and T. Zhou. (2021). *Future Global Climate: Scenario-Based Projections and Near-Term Information. In Climate Change 2021: The Physical Science Basis. Contribution of Working Group I to the Sixth Assessment Report of the Intergovernmental Panel on Climate Change*. [Masson-Delmotte, V., P. Zhai, A. Pirani, S.L. Connors, C. Péan, S. Berger, N. Caud, Y. Chen, L. Goldfarb, M.I. Gomis, M. Huang, K. Leitzell, E. Lonnoy, J.B.R. Matthews, T.K. Maycock, T. Waterfield, O. Yelekçi, R. Yu, B. Zhou(eds.)] Cambridge University Press, Cambridge United Kingdom, and New York, NY, USA, pp. 553–672, doi:10.1017/9781009157896.006.

Lowe, J. A. and J. M. Gregory (2006). "Understanding projections of sea level rise in a Hadley Centre coupled climate model". In: *Journal of Geophysical Research: Oceans* 111.C11.

Lyu, K., X. Zhang, and J. A. Church (2020). "Regional dynamic sea level simulated in the CMIP5 and CMIP6 models: Mean biases, future projections, and their linkages". In: *Journal of Climate* 33.15, pp. 6377–6398.

Mielke, C, E Frajka-Williams, and J. Baehr (2013). "Observed and simulated variability of the AMOC at 26 N and 41 N". In: *Geophysical Research Letters* 40.6, pp. 1159–1164.

Oppenheimer, M, B Glavovic, J Hinkel, R Van de Wal, A. Magnan, A Abd-Elgawad, R Cai, M Cifuentes-Jara, R. Deconto, T Ghosh, et al. (2019). "Sea level rise and implications for low-lying islands, coasts and communities, IPCC Special Report on the Ocean and Cryosphere in a Changing Climate, edited by: Pörtner, H.-O., Roberts, DC". In: *Intergov. Panel Clim. Change*.

O'Neill, B. C., E. Kriegler, K. Riahi, K. L. Ebi, S. Hallegatte, T. R. Carter, R. Mathur, and D. P. van Vuuren (2014). "A new scenario framework for climate change research: the concept of shared socioeconomic pathways". In: *Climatic change* 122.3, pp. 387–400.

Palmer, M. D., G. R. Harris, and J. M. Gregory (2018). "Extending CMIP5 projections of global mean temperature change and sea level rise due to thermal expansion using a physically-based emulator". In: *Environmental Research Letters* 13.8, p. 084003.

Palmer, M., J. M. Gregory, M. Bagge, D Calvert, J. Hagedoorn, T Howard, V Klemann, J. Lowe, C. Roberts, A. Slangen, et al. (2020). "Exploring the drivers of global and local sea-level change over the 21st century and beyond". In: *Earth's Future* 8.9, e2019EF001413.

Perrette, M, F Landerer, R Riva, K. Frieler, and M Meinshausen (2013). "A scaling approach to project regional sea level rise and its uncertainties". In: *Earth System Dynamics* 4.1, pp. 11–29.

Slangen, A., J. A. Church, C. Agosta, X. Fettweis, B. Marzeion, and K. Richter (2016). "Anthropogenic forcing dominates global mean sea-level rise since 1970". In: *Nature Climate Change* 6.7, pp. 701–705.

Sohail, T., B. Gayen, and A. M. Hogg (2020). "The dynamics of mixed layer deepening during open-ocean convection". In: *Journal of Physical Oceanography* 50.6, pp. 1625–1641.

Stammer, D., A. Cazenave, R. M. Ponte, and M. E. Tamisiea (2013). "Causes for contemporary regional sea level changes". In: *Annual review of marine science* 5, pp. 21–46.

Steffelbauer, D. B., R. E. Riva, J. S. Timmermans, J. H. Kwakkel, and M. Bakker (2022). "Evidence of regional sea-level rise acceleration for the north sea". In: *Environmental Research Letters*.

Tebaldi, C. and J. M. Arblaster (2014). "Pattern scaling: Its strengths and limitations, and an update on the latest model simulations". In: *Climatic Change* 122.3, pp. 459–471.

Van Vuuren, D. P., J. Edmonds, M. Kainuma, K. Riahi, A. Thomson, K. Hibbard, G. C. Hurtt, T. Kram, V. Krey, J.-F. Lamarque, et al. (2011). "The representative concentration pathways: an overview". In: *Climatic change* 109.1, pp. 5–31.

Yuan, J. and R. E. Kopp (2021). "Emulating Ocean Dynamic Sea Level by Two-Layer Pattern Scaling". In: *Journal of Advances in Modeling Earth Systems* 13.3, e2020MS002323.

Zanna, L., S. Khatiwala, J. M. Gregory, J. Ison, and P. Heimbach (2019). "Global reconstruction of historical ocean heat storage and transport". In: *Proceedings of the National Academy of Sciences* 116.4, pp. 1126–1131.

Zelinka, M. D., T. A. Myers, D. T. McCoy, S. Po-Chedley, P. M. Caldwell, P. Ceppi, S. A. Klein, and K. E. Taylor (2020). "Causes of higher climate sensitivity in CMIP6 models". In: *Geophysical Research Letters* 47.1, e2019GL085782.

Data Sources

Climate Explorer (n.d.). https://climexp.knmi.nl/start.cgi. (Accessed on 06/26/2022).

Frederikse, T., F. Landerer, L. Caron, S. Adhikari, D. Parkes, V. W. Humphrey, S. Dangendorf, P. Hogarth, L. Zanna, L. Cheng, and Y.-H. Wu (June 2020a). *data supplement of "The causes of sea-level rise since 1900"*. DOI: 10.5281/zenodo.3862995.

Met Office Hadley Centre observations datasets (n.d.). https://www.metoffice.gov.uk/hadobs/hadcrut5/data/current/download.html. (Accessed on 05/01/2022).

Ocean and Climate (n.d.). http://www.ocean.iap.ac.cn/pages/dataService/dataService.html?languageType=en&navAnchor=dataService. (Accessed on 06/13/2022).

Ocean Reanalysis of the 20th Century — ECMWF (n.d.). https://www.ecmwf.int/en/forecasts/dataset/ocean-reanalysis-20th-century. (Accessed on 01/04/2022).

Sea Level Projection Tool – NASA Sea Level Change Portal (n.d.). https://sealevel.nasa.gov/ipcc-ar6-sea-level-projection-tool?type=global. (Accessed on 15/03/2022).

A Projections of Predictor Variables: GSAT, GMTSL, and AMOC

Figure A.1 the CMIP5 and CMIP6 projections of GSAT, GMTSL, and AMOC for each scenario. The median and 5 – 95 percentile is plotted. For GSAT and GMTSL, the observations and AR6 ranges are plotted on top of the CMIP projections to compare. We see that the AR6 range of GSAT is lower than CMIP6, and higher than CMIP5 for the low and intermediate emission scenario. For the high emission scenario, the CMIP5 models agree with the AR6 assessed range. The CMIP6 models overestimate the range however. For GMTSL, we see that the CMIP5 and CMIP6 models show similar results, apart from the uncertainty band being wider for CMIP6. The AR6 assessed ranges are slightly larger than the model projections from CMIP5 and CMIP6, especially for the lower and intermediate scenario. For AMOC, we see that both ensembles project a weakening at the end of the 21st century. For the lower and intermediate emission scenario we see that the spread increased between CMIP5 and CMIP6.

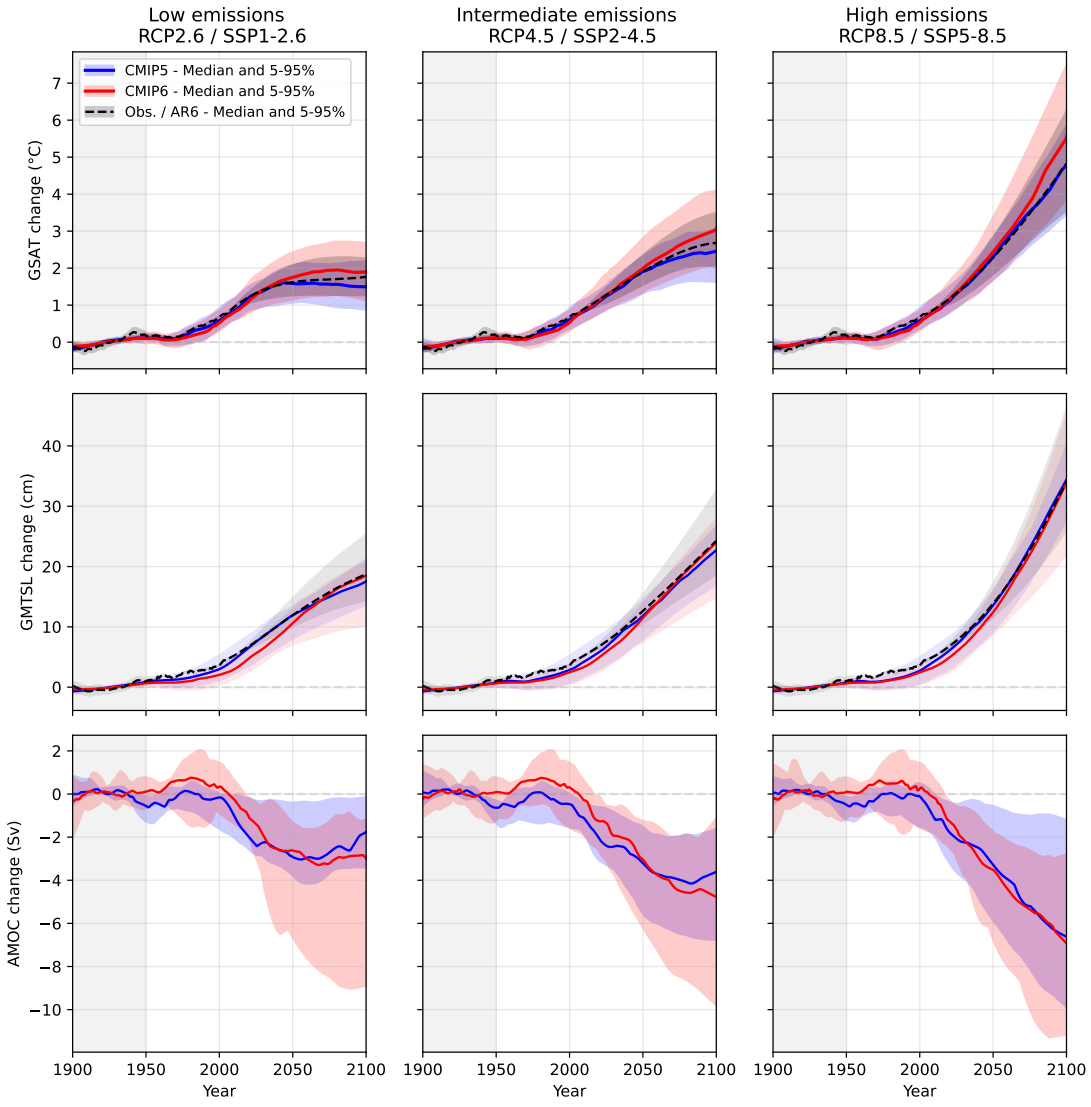

Figure A.1: Projections of GSAT, GMTSL, and AMOC from CMIP5 and CMIP6 models for different scenarios. The median and 5 - 95 percentile is shown. For GSAT and GMTSL, the concatenated time series of the observations with the AR6 assessed ranges are plotted in black.

B CMIP Models

The CMIP5 and CMIP6 climate models used in this study are listed in Tabel B.1 and B.2.

	Model I	**Model II**	**Model III**	**MLD analysis**
	GSAT	GSAT + GMTSL	GSAT + AMOC	
ACCESS1-0	X	X		X
CCSM4	X	X	X	
CMCC-CM	X	X		
CMCC-CMS	X	X		
CNRM-CM5	X	X	X	X
CSIRO-Mk3-6-0	X	X		X
CanESM2	X	X		
EC-EARTH	X			
GFDL-ESM2G	X			
GFDL-ESM2M	X			X
GISS-E2-R	X	X	X	
HadGEM2-CC	X	X		
HadGEM2-ES	X	X		
IPSL-CM5A-LR	X	X		
IPSL-CM5A-MR	X	X		
IPSL-CM5B-LR	X			
MIROC-ESM	X	X		
MIROC-ESM-CHEM	X	X		
MIROC5	X	X	X	
MPI-ESM-LR	X	X	X	X
MPI-ESM-MR	X	X	X	X
MRI-CGCM3	X	X	X	X
NorESM1-M	X	X	X	X
NorESM1-ME	X	X	X	X
bcc-csm1-1	X	X		
bcc-csm1-1-m	X	X		
inmcm4	X	X		

Table B.1: Selection of 27 CMIP5 models used in this study. The X denotes for which analysis they were included.

	Model I	**Model II**	**Model III**	**MLD analysis**
	GSAT	GSAT + GMTSL	GSAT + AMOC	
ACCESS-CM2	X	X	X	X
ACCESS-ESM1-5	X	X	X	X
BCC-CSM2-MR	X			X
CAMS-CSM1-0	X			X
CESM2	X			X
CESM2-WACCM	X		X	X
CIESM	X			
CMCC-CM2-SR5	X	X	X	X
CNRM-CM6-1	X	X		X
CNRM-ESM2-1	X	X		X
CanESM5	X	X	X	X
CanESM5-CanOE	X	X		X
EC-Earth3	X	X		X
EC-Earth3-Veg	X	X		X
FGOALS-g3	X		X	X
GFDL-ESM4	X		X	X
GISS-E2-1-G	X			X
HadGEM3-GC31-LL	X	X		X
HadGEM3-GC31-MM	X			X
INM-CM4-8	X	X	X	
INM-CM5-0	X	X	X	
IPSL-CM6A-LR	X	X	X	X
MIROC-ES2L	X			
MIROC6	X	X	X	X
MPI-ESM1-2-HR	X	X	X	X
MPI-ESM1-2-LR	X	X	X	X
MRI-ESM2-0	X	X	X	X
NESM3	X			X
NorESM2-LM	X	X	X	X
NorESM2-MM	X	X		X
UKESM1-0-LL	X	X		X

Table B.2: Selection of 31 CMIP6 models used in this study. The X denotes for which analysis they were included.

C Linear Regression for Individual Models

The figures included in this Appendix show the regression results for the individual CMIP models. The RMSE and the coefficient of determination, R^2, is shown in the title. The regression coefficients are given for all single models. Overall, we see that R^2 is large for most models showing a substantial change in ODSL. For models that show little change, the R^2 score is small. Figures C.1, and C.2 show the results for Model I, Figures C.3, and C.4 show the results for Model II, and Figures C.5, and C.6 show the results for Model III. For Model II, we see that some models show a positive contribution from one of the predictor variables and a negative contribution from the other. As was discussed in Section 5, physically this does not make sense since GSAT and GMTSL are positively correlated. However, for some models the error is minimised, thus the shape of the CMIP data is best resembled, when a positive contribution of one predictor variable is taken and a negative for the other. This is thus due to optimisation of the regression model.

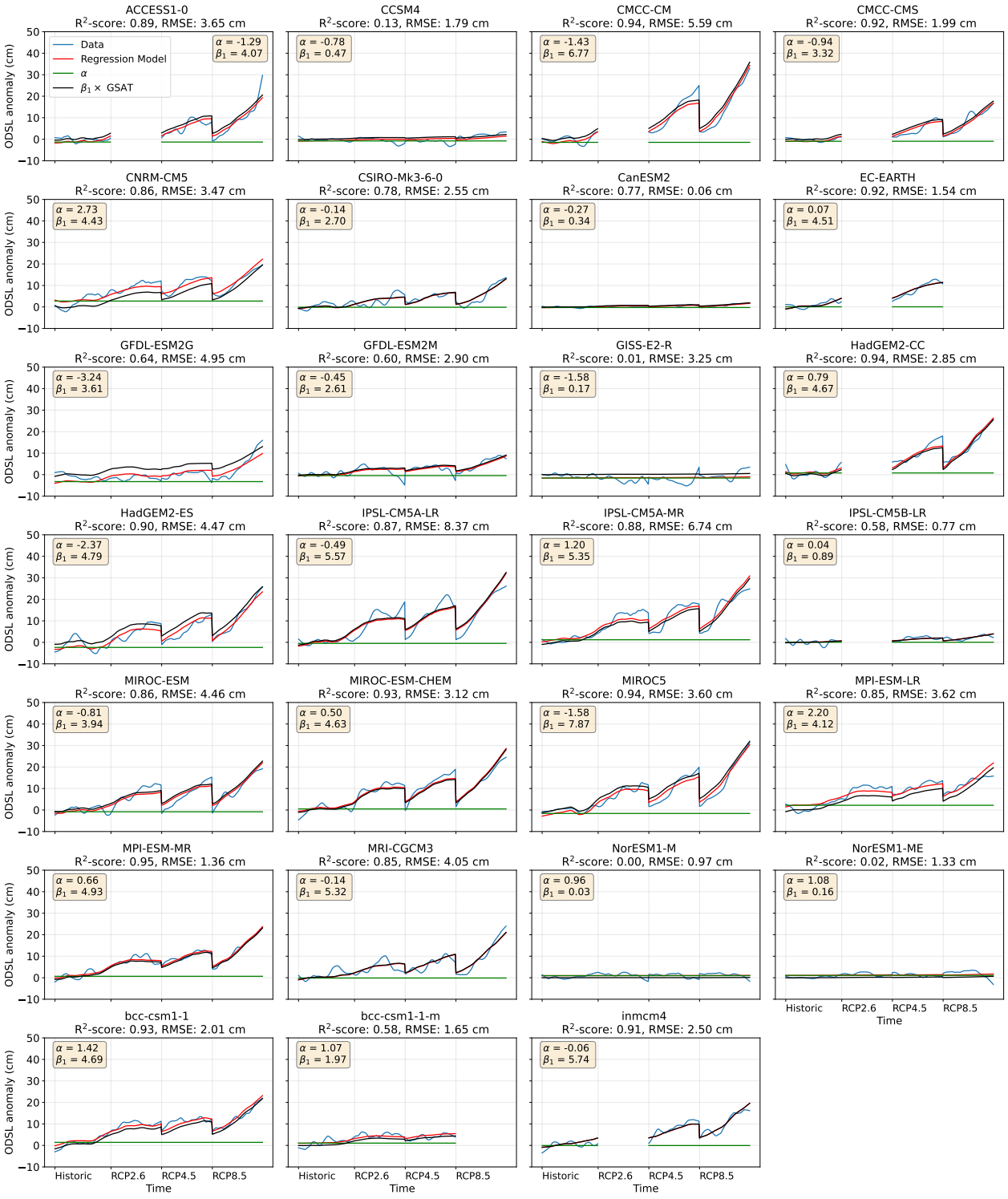

Figure C.1: CMIP5 individual model results for the regression analysis using regression Model I with GSAT as predictor variable.

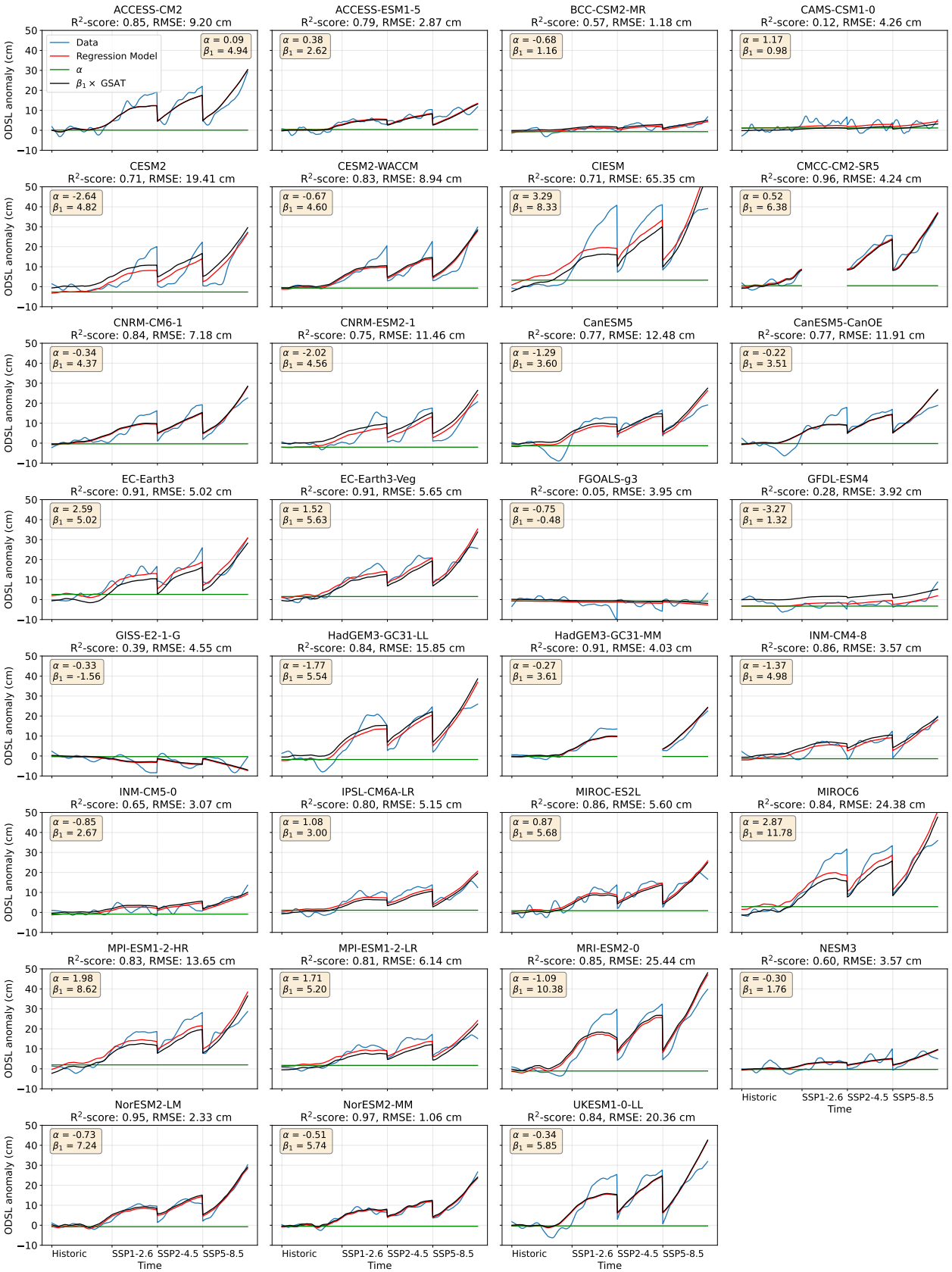

Figure C.2: CMIP6 individual model results for the regression analysis using regression Model I with GSAT as predictor variable.

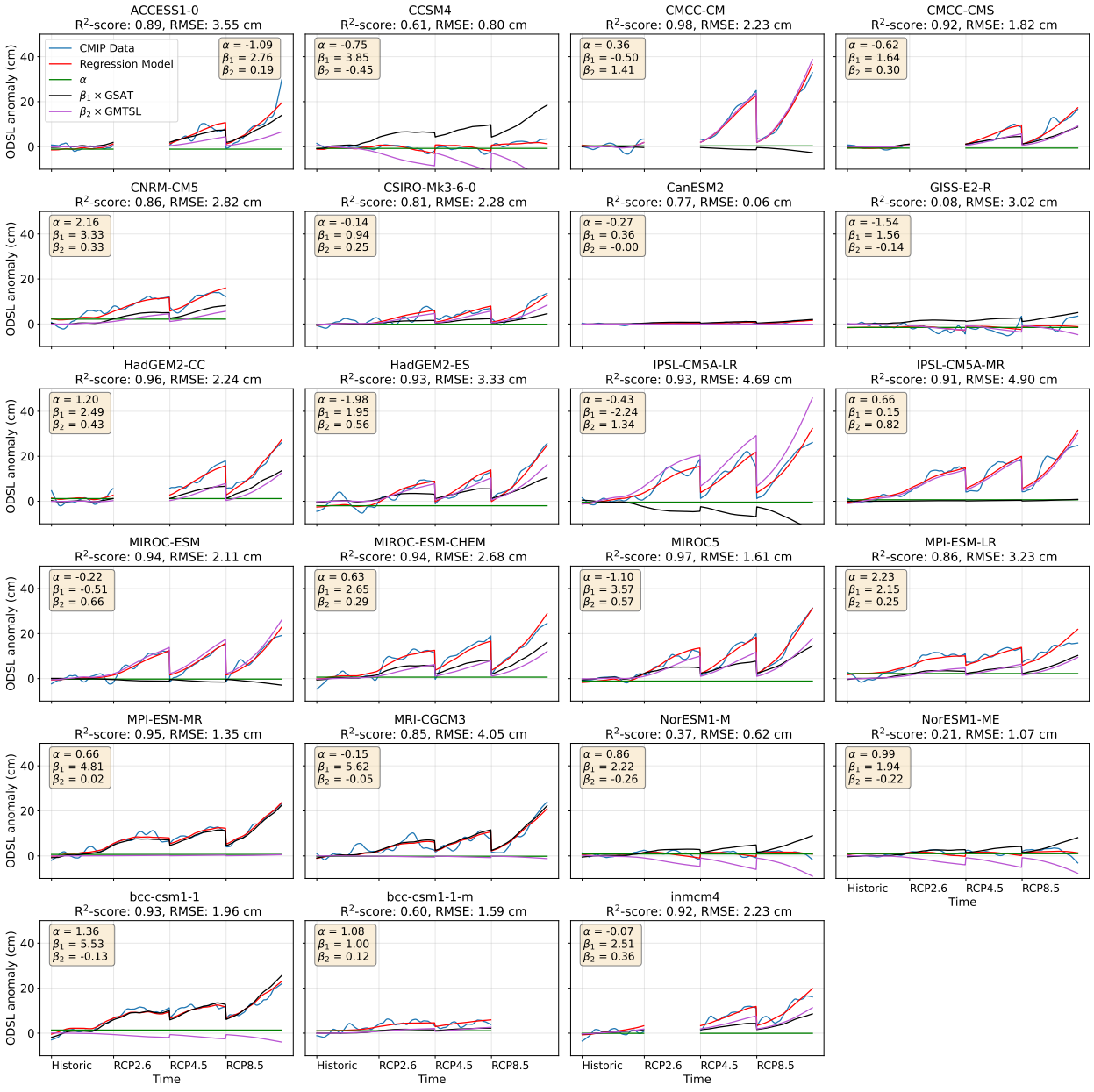

Figure C.3: CMIP5 individual model results for the regression analysis using regression Model II with GSAT and GMTSL as predictor variables.

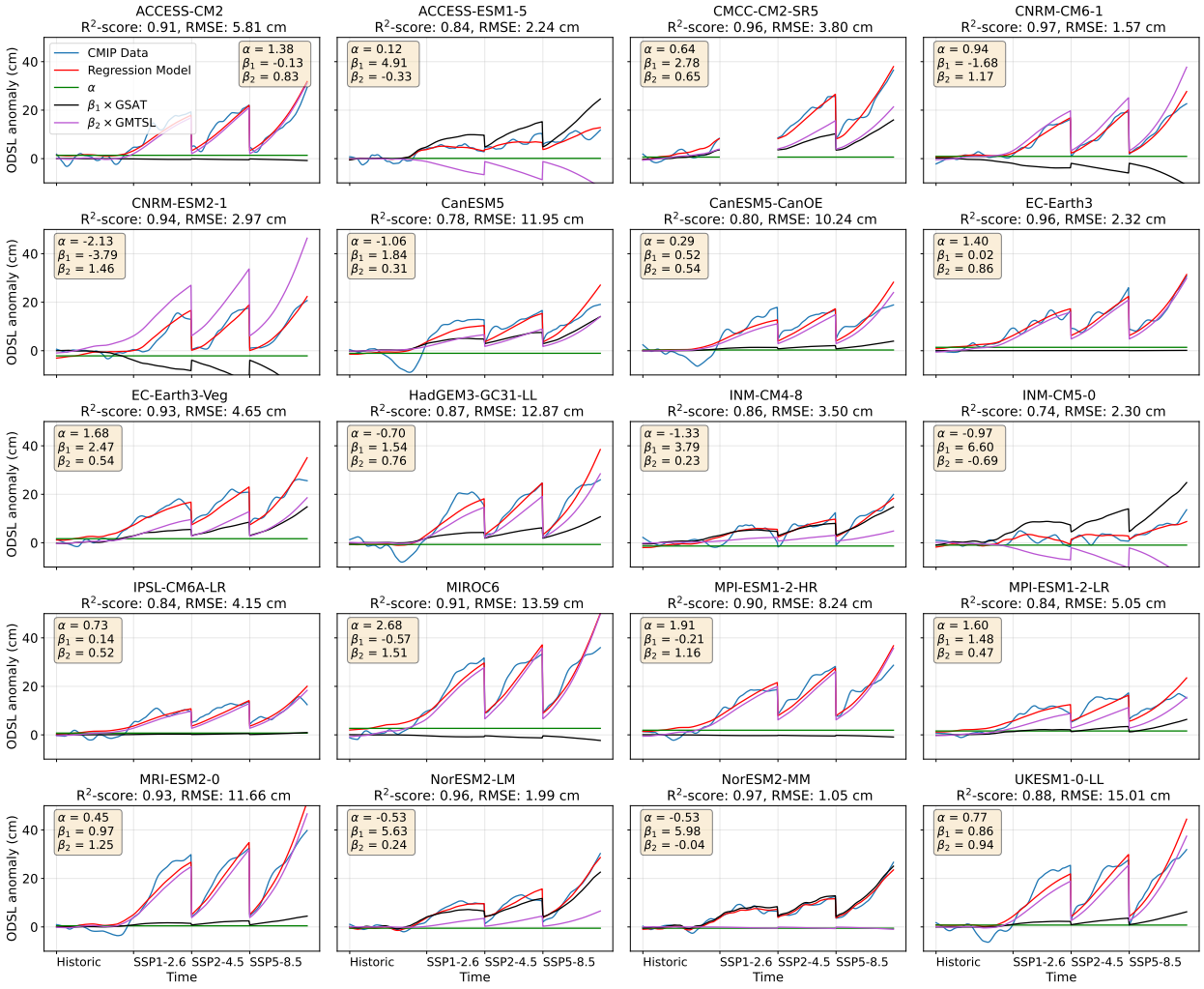

Figure C.4: CMIP6 individual model results for the regression analysis using regression Model II with GSAT and GMTSL as predictor variables.

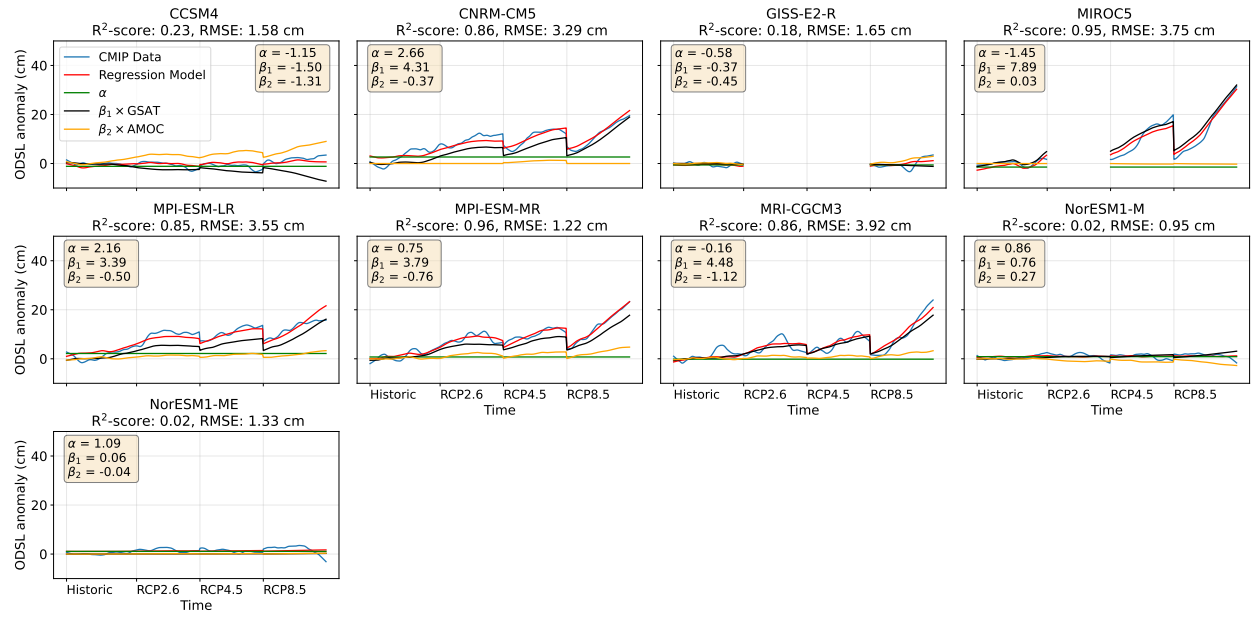

Figure C.5: CMIP5 individual model results for the regression analysis using regression Model III with GSAT and AMOC as predictor variables.

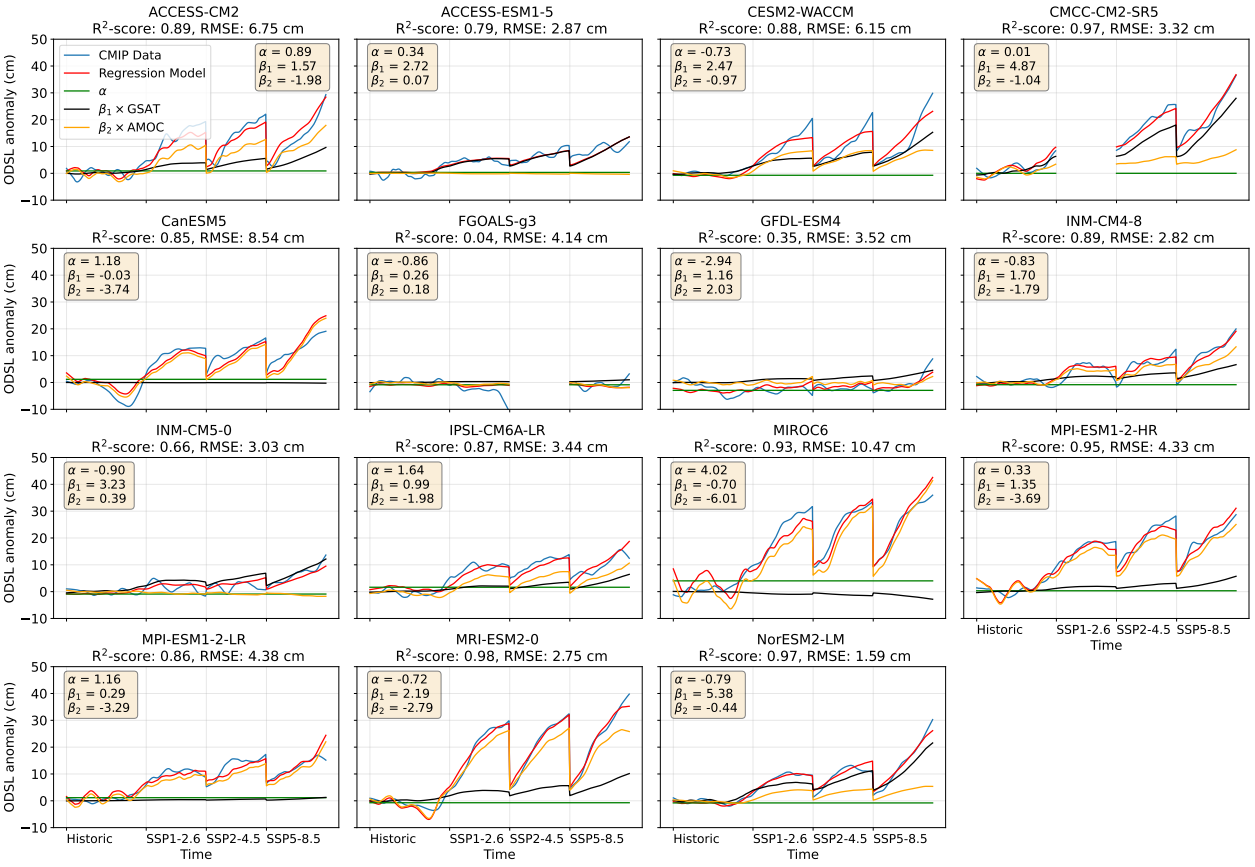

Figure C.6: CMIP6 individual model results for the regression analysis using regression Model III with GSAT and AMOC as predictor variables.

D Influence of the Smoothing Window

In this study, we used a 25-year smoothing window to focus on on long term changes in the different climate variables. We repeated the analysis with the original unsmoothed data, and data with a 10-year smoothing filter applied. Figure D.1 shows the results of the the analysis for Model III. with predictor variables GSAT and AMOC. Here, we see that the relative importance of AMOC increases when increasing the smoothing window for CMIP6. This might indicate that the AMOC is more important on longer time scales. The effect is less apparent for CMIP5.

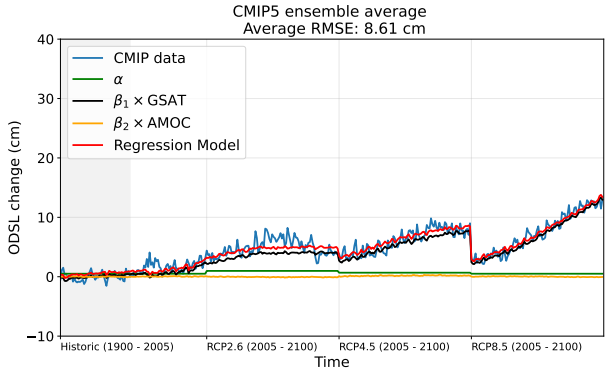

(a) CMIP5: No smoothing

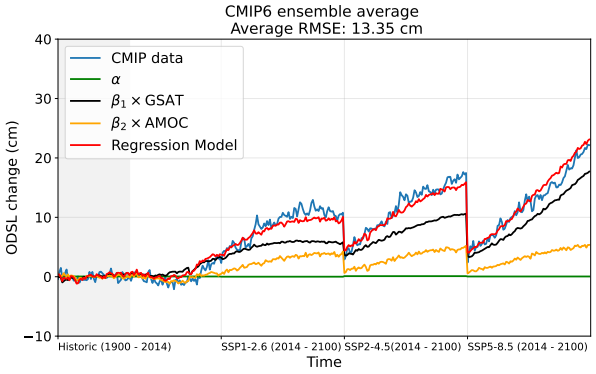

(b) CMIP6: No smoothing

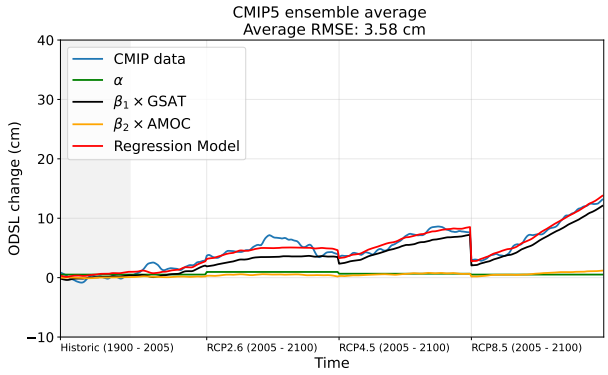

(c) CMIP5: 10-yr smoothing

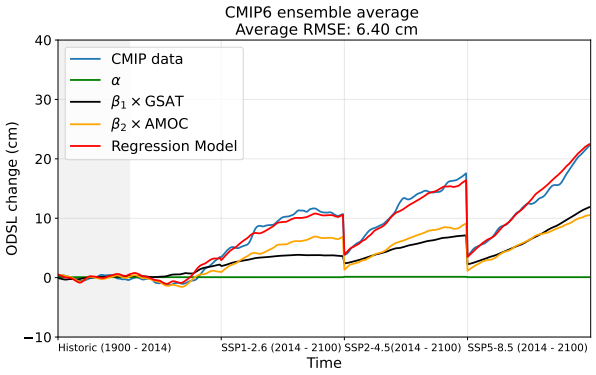

(d) CMIP6: 10-yr smoothing

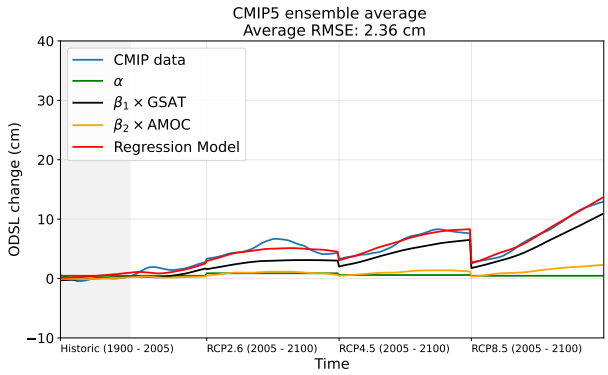

(e) CMIP5: 25-yr smoothing

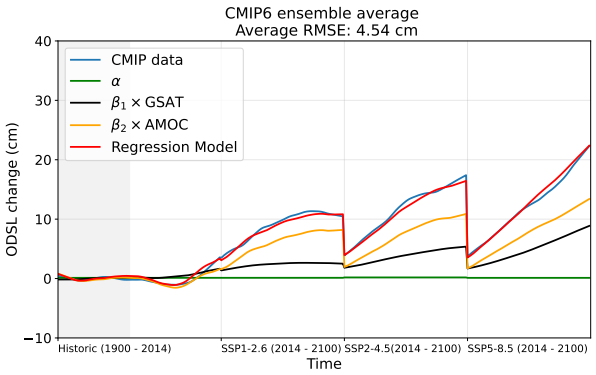

(f) CMIP6: 25-yr smoothing

Figure D.1: Ensemble averaged regression for Model III. Results are shown for CMIP5 (left) and CMIP6 (right) with different smoothing filters applied.

E Mixed Layer Depth for Individual Models

Figure E.1 shows the MLD for the models that we include in our study. This is the selection of models that also has data available for ODSL and GSAT. Some models show a deeper mixed layer in multiple regions. The NorESM2 models show a relatively shallow mixed layer in CMIP5, however in CMIP6 the models show a deep mixed layer in all three defined regions.

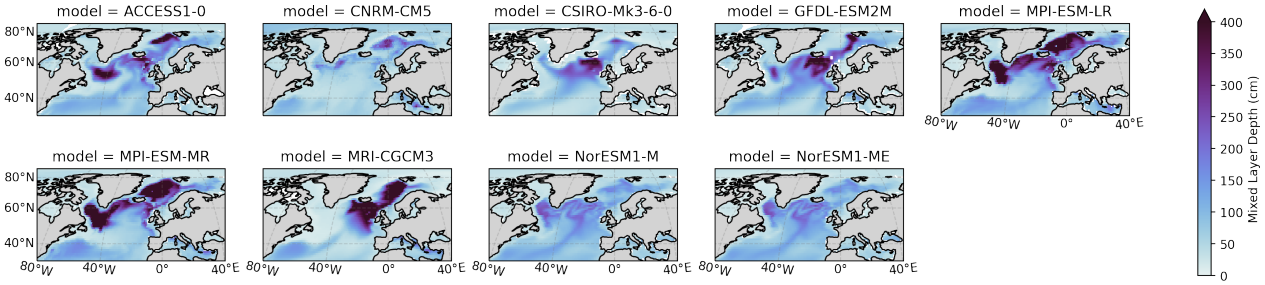

(a) CMIP5

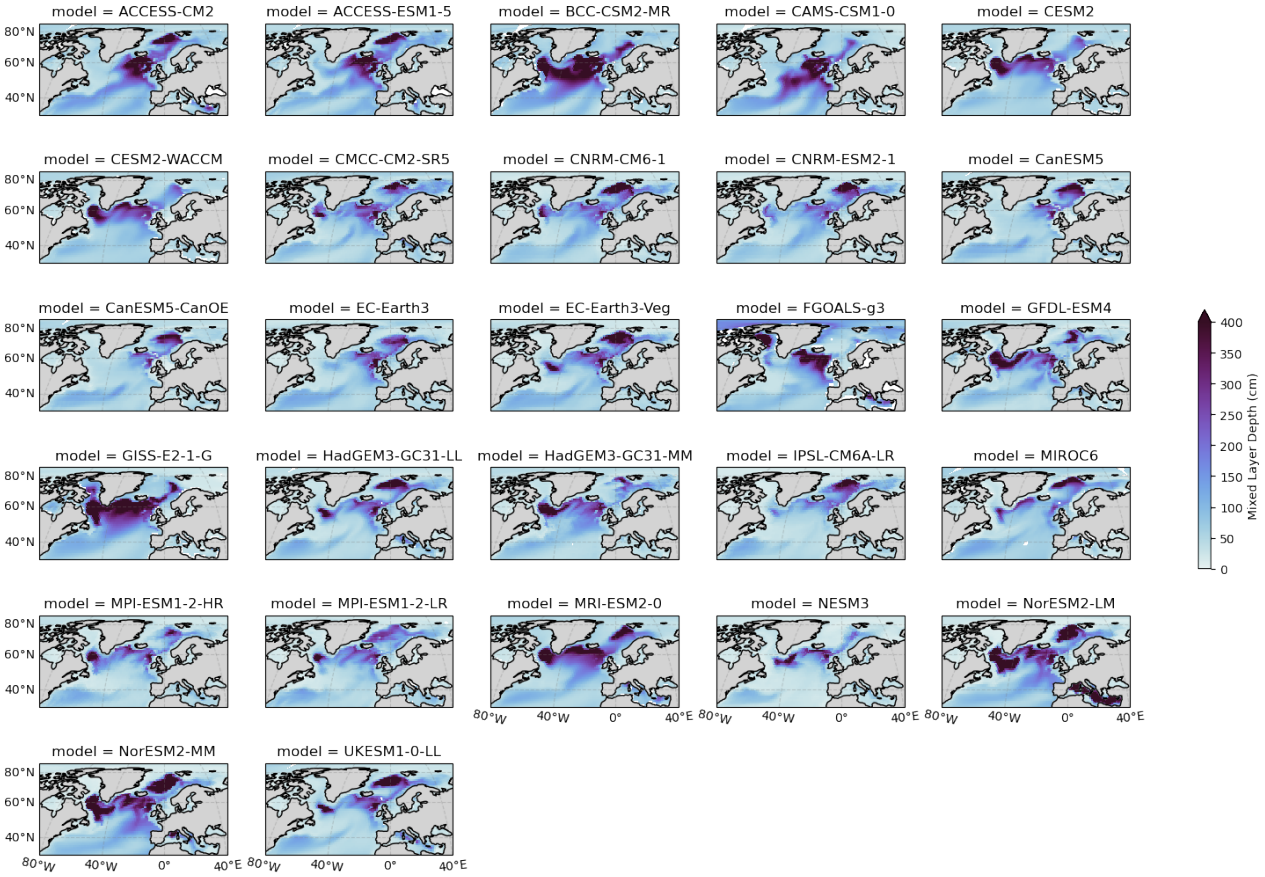

(b) CMIP6

Figure E.1: Mixed layer depth (MLD) averaged over 1975 – 2004 for individual CMIP5 (a) and CMIP6 (b) models included in our analysis.

F Python Code

The code that was used for the data analysis and figures in this thesis can be accessed via:
`https://github.com/FrankaJes/Thesis_KNMI`